CHALMERS

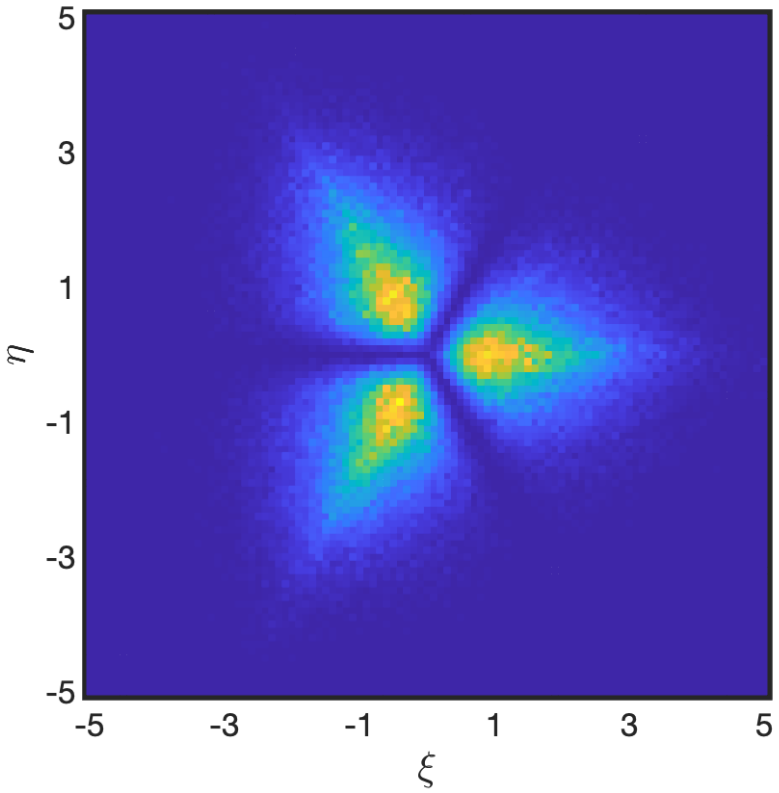

Patterns in Interacting Quantum Gases

Exploring pairing effects, magic numbers, and Pauli crystals

Bachelor's thesis in Engineering Physics

Bekassy Viktor, Heuts Olivia, Lech Alex,
Lundqvist Carin, Magnusson Erik

DEPARTMENT OF PHYSICS

CHALMERS UNIVERSITY OF TECHNOLOGY, UNIVERSITY OF GOTHENBURG
Gothenburg, Sweden 2021
www.chalmers.se

Bachelor's thesis 2021

Patterns in Interacting Quantum Gases

Exploring pairing effects, magic numbers, and Pauli crystals

Viktor Bekassy
Olivia Heuts
Alex Lech
Carin Lundqvist
Erik Magnusson

GÖTEBORGS
UNIVERSITET

Department of Phyiscs
Chalmers University of Technology, University of Gothenburg
Gothenburg, Sweden 2021

Patterns in Interacting Quantum Gases
Exploring pairing effects, magic numbers, and Pauli crystals
Viktor Bekassy, Olivia Heuts, Alex Lech, Carin Lundqvist and Erik Magnusson

Supervisor: Dr. Johannes Hofmann, Department of Physics
Examiners: Jan Swenson and Martina Ahlberg, Department of Physics

Bachelor's Thesis 2021
Department of Physics
Chalmers University of Technology
University of Gothenburg
SE-412 96 Gothenburg
Telephone +46 31 772 1000

Cover: A histogram showing a Pauli crystal in 2D for three particles constructed in Matlab. The picture is derived and discussed in chapter 5.

Typeset in LaTeX
Printed by Chalmers Reproservice
Gothenburg, Sweden 2021

Patterns in Interacting Quantum Gases
Exploring pairing, magic numbers, and Pauli crystals
Viktor Bekassy, Olivia Heuts, Alex Lech, Carin Lundqvist and Erik Magnusson
Department of Physics
Chalmers University of Technology
University of Gothenburg

Abstract

Quantum gases is a novel field of experimental research, where it is possible to study the universal behaviour of quantum particles under controlled circumstances. In two experiments by Zürn *et al.* and Holten *et al.*, patterns such as paring effects, magic numbers and Pauli crystals have emerged in a quantum gas consisting of a few ultracold ^{6}Li atoms confined in an optical trap. By modelling these experiments and using the universal behaviour of quantum particles, we can achieve a greater understanding of how the building blocks of our universe behave and then apply that knowledge to more complicated systems, such as neutron stars or the atomic nucleus. This thesis aims to model the mentioned experiments as a few interacting fermions in a harmonic potential. By treating the interaction as a minor perturbation and calculating the energy of the system numerically with perturbation theory, we were able to compare our results with the experiments by Zürn *et al.* and found that they were in good agreement. Both showed a pronounced shell structure, resulting in magic numbers, and the emergence of pairing between fermions. Furthermore, the results were consistent with our analytically derived solution for two particles. Additionally, Pauli crystals in one and two dimensions were simulated using Matlab and the Metropolis algorithm, resulting in us successfully recreating the very recent experimental results by Holten *et al.*. Finally, interactions were added to Pauli crystals in 1D, showing new pairing patterns and opening up for further research.

Keywords: Quantum gas, Fermi gas, Fermions, Magic numbers, Pauli crystals, Separation energy, Perturbation theory

Sammandrag

Kvantgaser är ett intressant område för experimentell forskning där det är möjligt att studera det unviersalla beteendet hos kvantpartiklar under kontrollerade omständigheter. I experiment av Zürn *et al.* och Holten *et al.* har mönster såsom pareffekter, magiska tal och paulikristaller observerats i kvantgaser bestående av ett fåtal ultrakalla ^{6}Li atomer fångade i en optisk fälla. Genom att modellera dessa experiment och utnyttja det universella bettende hos kvantpartiklar är det möjligt att få en djupare förståelse för hur universums byggstenar fungerar och sedan applicera den kunskapen på mer komplicerade system, såsom neutronstjärnor och atomkärnor. I det här arbetet avser vi modellera de nämnda experimenten som ett fåtal interagerande fermioner i en harmonisk potential. Genom att behandla interaktionen som en mindre störning och beräkna systemets energi numeriskt med störningsteori, kunde vi jämföra våra resultat med experimenten av Zürn *et al.* och fann att de stämde väl överens. Båda visade en tydlig skalstruktur som resulterade i magiska tal och uppkomsten av parbeteende mellan fermioner. Vidare var resultaten konsistenta med den härledda analytiska lösningen för två partiklar. Därtill simulerades paulikristaller i en och två dimensioner med hjälp av Matlab och Metropolisalgoritmen, som resulterade i att vi framgångsrikt återskapade fjolårets resultat i Holten *et al.*. Slutligen, undersöktes paulikristaller med interaktioner i 1D, som visade nya parningsmönster och öppnar upp för mer framtida forskning.

Nyckelord: Kvantgas, Fermigas, Fermioner, Magiska tal, Paulikristaller, Separationsenergi, Störningsteori

Acknowledgements

We would like to extend our grand gratitude to Johannes Hofmann and the endless well of wisdom that is his mind. Dr. Hofmann has been a constant presence on the journey that has been the creation of this thesis. A comment of encouragement in fruitful times, a hopeful email in the darkest hour. Taking on the role of a guide on this expedition within the field of quantum gases, he has led us around potential traps and barely distinguishable obstacles. Dominating the field. He is not the mentor we deserved, but the mentor we needed.

This road has not been without trials and luckily it is not one we have had to take alone. We are fortunate and incredibly thankful for the researchers who sent us their data, enabling us to verify our results and reach the finish line: Dr. Zürn, Dr. D'Amico, and Marvin Holten.

Ultimately, we are grateful towards our families and friends supporting us throughout these trying times. It has not merely been a voyage through science, but also within life itself.

Viktor Bekassy, Olivia Heuts, Alex Lech, Carin Lundqvist
and Erik Magnusson, Gothenburg, May 2021

Contents

Part I

A Swedish Summary of the Thesis

Mönster i interagerande kvantgaser

Bakgrund

En kvantgas är en fas hos ett partikelsystem som uppkommer antingen vid extremt höga densiteter, såsom återfinns i en neutronstjärna, eller vid väldigt låga temperaturer runt absoluta nollpunkten. Partiklarnas låga rörelsemängd gör att deras position smetas ut enligt Heisenbergs osäkerhetsprincip, vilket leder till att deras de Broglie-våglängder överlappar och att kvanteffekter tar över [1]. Det har på senare årtionden uppkommit forskningfält som studerar dessa kvantgaser i optiska fällor. En anledning till detta är att det universella beteendet hos kvantpartiklar gör att modeller som utvecklas för system med endast ett fåtal partiklar kan tillämpas på mer komplicerade system som neutronstjärnor och atomkärnor. Kvantgaser som består av fermioner, Fermigaser, är av extra betydelse då fermioner som exempelvis elektroner och nukleoner utgör materia och därför kan ge oss en djupare förståelse för världens uppbyggnad. Vidare uppvisar de intressanta mönster på grund av pauliprincipen, som dikterar att fermioner inte kan befinna sig i samma tillstånd och alltså inte uppta samma plats i rummet [4].

I det här arbetet avser vi att teoretiskt återskapa två experiment, Zürn *et al.* [2] och Holten *et al.* [3], som gjort mätningar på interagerande Fermigaser bestående av ett fåtal partiklar fångade i en harmonisk potential nära absoluta nollpunkten. Genom att modellera dessa experiment är målet att finna en överenskommelse mellan vår modell och experimenten samt undersöka mönstrena som uppkommer i Fermigaser. Först undersöker vi mönster mellan stabiliteten hos systemet och vissa "magiska" tal av partiklar och sedan de geometriska strukturerna kända som paulikristaller, som uppkommer på grund av pauliprincipen.

Teori

För att förstå ett system med många interagerande partiklar krävs det det först en förståelse för den enskilda partikeln. På kvantskalan beskrivs partiklens tillstånd av dess vågfunktion $\psi(x)$. Vid observation kollapsar vågfunktionen till en partikel enligt dess sannolikhetsfördelning $\left|\psi(x)\right|^2$. Vågfunktionen ges av den stationära Schrödingerekvationen $\hat{H}(x)\psi(x) = E\psi(x)$ med Hamiltonianen $\hat{H}$ och partikelenergin E. I vår modell befinner sig partiklarna i en kvantharmonisk oscillator som har Hamiltonianen

$$\hat{H}_{QHO}(x) = \frac{\hat{p}^2}{2m} + \frac{1}{2}m\omega^2\hat{x}^2 = -\frac{\hbar^2}{2m}\frac{d^2}{dx^2} + \frac{1}{2}m\omega^2x^2, \tag{0.1}$$

där m är partikelmassan, ω oscillatorns karaktäristiska vinkelfrekvens och x positionen. Den första termen är partikelns kinetiska energi, och den andra den omgivande potentialen $V(x)$. Den karakteristiska längdskalan för kvantharmoniska oscillatorn är oscillatorlängden $l_{ho} = \sqrt{\hbar/m\omega}$, och den karakteristiska energin är $\hbar\omega$. Vågfunktionen på dimensionslös form med huvudkvanttalet n ges som

$$\widetilde{\psi}_n(\xi) = \sqrt{l_{ho}} \cdot \psi_n(\xi) = \frac{1}{\sqrt{2^n n!}}\frac{1}{\pi^{\frac{1}{4}}}e^{-\frac{\xi^2}{2}}H_n\left(\xi\right), \tag{0.2}$$

med den tillhörande energin $E_n = \hbar\omega\left(n + \frac{1}{2}\right)$ som också kan göras dimensionslös genom att dividera med den karaktäristiska energin $\hbar\omega$. Grundtillståndet hos en endimensionell

kvantharmonisk oscillator är när kvanttalet $n = 0$, vilket motsvarar energin $\hbar\omega/2$.

För flera partiklar blir den totala Hamiltonianen summan av de enskilda partiklarnas Hamiltonianer. Likartat är vågfunktionen för urskiljbara partiklar produkten av de enskilda partiklarnas vågfunktioner. Men fermioner av samma spinn går inte att urskilja från varandra och är dessutom antisymmetriska under utbyte. Alltså måste den totala vågfunktionen för N partiklar beskrivas med den så kallade Slaterdeterminanten, som tar hänsyn till antisymmetrin. Slaterdeterminanten skrivs på kompakt form som

$$\Psi_{n_1,...,n_N}(x_1, x_2, ..., x_N) = \frac{1}{\sqrt{N!}} \sum_{p \in S_N} \text{sign}(p) \left(\prod_{j=1}^{N} \psi_{n_{p(j)}}(x_j) \right). \tag{0.3}$$

$1/\sqrt{N!}$ är en normaliseringskonstant, x_i positionen för partikeln numrerad i och n_i visar ett ockuperat tillstånd. Vidare är S_N permutationsgruppen för N, som innehåller alla möjliga permutationer p av N komponenter, och $\text{sign}(p) = \pm 1$ beroende på om permutionen p är jämn eller udda. I ett system med fler spinnkomponenter multipliceras Slaterdeterminanterna för alla spinnkomponenter, då partiklar med olika spinn är urskiljbara. Vidare är partiklar av olika spinn degenererade och kan ockupera samma energinivå.

Härledningar

För att kunna studera effekten av interaktioner på ett systems stabilitet beräknar vi energin för ett tillstånd med två spinn vi kallar upp, $\uparrow$, och ned, $\downarrow$, utan interaktioner. Denna blir

$$E = \hbar\omega \left(\frac{N}{2} + \sum_{i=1}^{N_\uparrow} n_{\uparrow i} + \sum_{j=1}^{N_\downarrow} n_{\downarrow j} \right), \tag{0.4}$$

där $N = N_\uparrow + N_\downarrow$ är det totala antalet partiklar, bestående av $N_\uparrow$ partiklar med spinn upp och $N_\downarrow$ partiklar med spinn ner. Detta resultatet säger att energin för ett tillstånd i ett icke-interagerande system är summan av de enskilda partiklarnas energier. Med det etablerat inför vi interaktioner mellan partiklar av olika spinn som modelleras med en deltafunktionspotential. Detta går bra eftersom den stora de Broglie-våglängden för kvantgaser kommer göra detaljerna hos den interagerande potentialen irrelevanta [11]. Den totala Hamiltonianen med interaktionstermen blir

$$\hat{H} = \sum_{i=1}^{N_\uparrow} \hat{H}_{QHO}(x_{\uparrow i}) + \sum_{j=1}^{N_\downarrow} \hat{H}_{QHO}(x_{\downarrow j}) + \sum_{i=1}^{N_\uparrow} \sum_{j=1}^{N_\downarrow} \alpha\delta(x_{\uparrow i} - x_{\downarrow j}), \tag{0.5}$$

där α är interaktionsstyrkan mellan två partiklar. För två partiklar med olika spinn kan energin som resulterar från ovanstående Hamiltonian tas fram analytiskt. Problemet har ett sedan tidigare känt svar i 1D, men vi härleder uttrycket själva genom att dela upp Hamiltonianen i en del för masscentrum och en relativ del. Masscentrum-delen ger energin för en vanlig harmonisk oscillator, medan den relativa delen ger sambandet mellan energin och den skalade interaktionsstyrkan $\beta = \alpha/l_{ho}\hbar\omega$ som

$$\beta(E) = -2\sqrt{2} \frac{\Gamma\left(-\frac{E}{2} + \frac{3}{4}\right)}{\Gamma\left(-\frac{E}{2} + \frac{1}{4}\right)}. \tag{0.6}$$

För att beräkna energin för det interagerande systemet med fler än två partiklar används störningsteori [4], då den analytiska lösningen blir för komplicerad. Korrektionerna till den ostörda energin fås genom att överlappsintegralen $\langle\Psi| \hat{H} |\Psi'\rangle$ beräknas. I vårt fall finns det bara fem olika fall för överlappsintegralen, vilket förenklar beräkningar och dessa redogörs för i tabell 0.1.

Fall	$\langle\Psi\|\hat{H}'\|\Psi'\rangle$
Fall 1:	$\frac{1}{l_{ho}}\sum_{i=1}^{N_\uparrow}\sum_{j=1}^{N_\downarrow}\int \mathrm{d}\xi\, \|\widetilde{\psi}_{n_i}(\xi)\|^2\|\widetilde{\psi}_{n_j}(\xi)\|^2$
Fall 2:	$\frac{1}{l_{ho}}\sum_{j=1}^{N_\downarrow}\int \mathrm{d}\xi\, \widetilde{\psi}^*_{n_\kappa}(\xi)\widetilde{\psi}_{n'_\lambda}(\xi)\|\widetilde{\psi}_{n_j}(\xi)\|^2$
Fall 3:	$\frac{1}{l_{ho}}\sum_{i=1}^{N_\uparrow}\int \mathrm{d}\xi\, \widetilde{\psi}^*_{n_\mu}(\xi)\widetilde{\psi}_{n'_\nu}(\xi)\|\widetilde{\psi}_{n_i}(\xi)\|^2$
Fall 4:	$\frac{1}{l_{ho}}\int \mathrm{d}\xi\, \widetilde{\psi}^*_{n_\kappa}(\xi)\widetilde{\psi}^*_{n'_\lambda}(\xi)\widetilde{\psi}_{n_\mu}(\xi)\widetilde{\psi}_{n'_\nu}(\xi)$
Annars:	0

Tabell 0.1: De fem fallen för överlappsintegralen beror på hur många ockuperade enpartikel-tillstånd n som skiljer sig åt mellan Ψ och Ψ'. Om Ψ och Ψ' är identiska blir det fall ett. Om de skiljer sig med ett ockuperad enpartikel-tillstånd med spinn upp eller spinn ner blir det fall två respektive fall tre. Om de skiljer sig med en ockuperad enpartikel-tillstånd i både upp- och nedspinnspartiklarna blir det fall fyra. Annars blir det fall fem.

Resultat och diskussion

Med hjälp av ovan nämnda fall av överlappsintegralen kan energin för ett interagerande system med flera spinn beräknas. Vid ultrakalla temperaturer befinner sig partiklarna för det mesta i systemets gruntillstånd [10, p. 277-278] och ett exempel för ett system med fyra spinn, både med och utan interaktioner, ses i figur 0.1a. Redan utan interaktioner observeras en tydlig skaleffekt, då lutning på grafen endast förändras vid multiplar av antalet spinn. Detta kan förklaras av att se energinivåerna i den harmoniska oscillatorn som skal, där ökningen i energi är konstant medan ett skal fylls med partiklar av olika spinn i 1D. När interaktionerna läggs på blir skaleffekten tydligare, och dessutom minskar systemets energi även inom ett skal. Mindre energi motsvarar ökad stabilitet; dessa tal kan jämföras med de magiska talen i 1D, som är det orsaken till att vissa nukleontal är mer stabila i kärnfysik.

För att jämföra resultaten med experimenten i [2] används storheten "separation energy" $E_{sep}(N)$, vilket är energin som frigörs när den N:te atomen tunnlar ut ur den begränsande potentialen och lämnar $N-1$ partiklar i grundtillståndet. Som kan ses i figur 0.1b matchar våra modeller med första och andra ordningens störningsteori beteendet hos den experimentella mätningen i [2] väl, och sammanfaller också bra med de teoretiska beräkningarna i [17]. Effekten i [2] där ett jämnt antal partiklar har större amplitud på separationsenergin, och därmed motsvarar ett stabilare system, syns tydligt i våra simuleringar och verfierar alltså vår modell. Vidare stämmer vår modell väl överens med den analytiska härledningen för två partiklar, vilket bekräftar att interaktionen får behandlas som en störning för små α. Att vår modell lyckas återskapa experiment i en dimension kan ses som grund för att generalisera modellen till högre dimensioner vid fortsatta studier.

Efter att ha studerat interagerande system, övergår vi till att studera mönstrena som uppkommer i icke-interagerande system på grund av pauliprincipen. Genom att utföra upprepade mätningar av ett fåtal fermioner och behandla mätningarna kommer särskilda mönster uppkomma som speglar denna princip, så kallade paulikristaller. Mönstrena mättes experimentellt förra året i [3] och vi har lyckats simulera dessa mätningar. Genom att använda Metropolisalgoritmen [21] väljer vi mätningar som har en realistisk spridning i sannolikhet $|\Psi|^2$. När varje mätnings masscentrum flyttas till origo syns det tydligt att deras vågfunktion kollapsar i enlighet med deras sannolikhetsfördelningen, som dock inte tar hänsyn till partiklarna positioner gentemot varandra. För att få en känsla för korrelationen mellan partiklar används istället en annan algoritm som beräknar partiklarnas mest sannolika positioner, då visar det sig att partiklarna lägger sig i cirkulära skal för att maximera deras inbördes avstånd. Se för sex partiklar i figur 0.2a. Med den informationen är det möjligt att ytterligare processera datan från Metropolisalgoritmen genom att

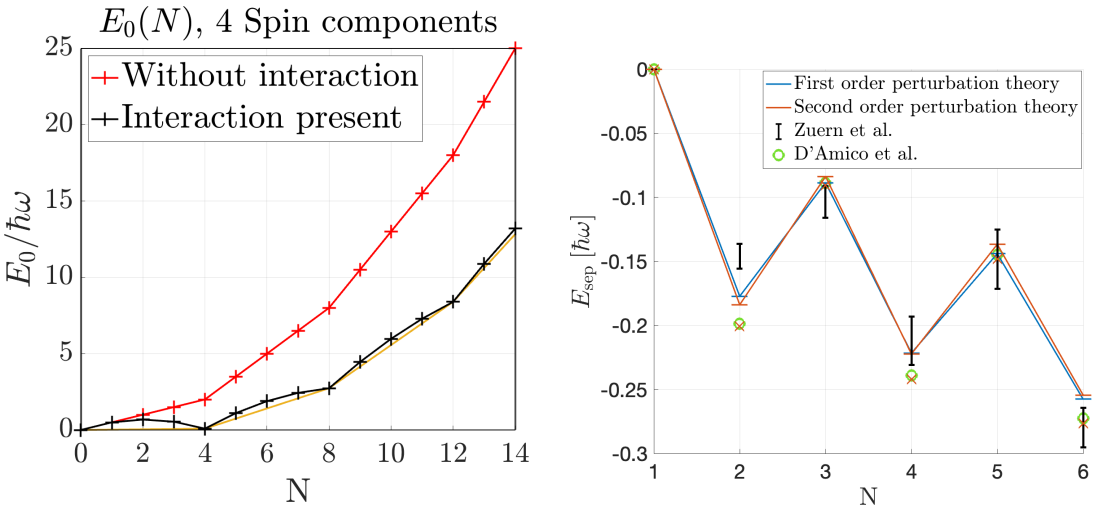

(a) **(b)**

Figur 0.1: **(a)** ger energin för ett system med fyra spinnkomponenter som uppvisar en tydlig skalstruktur. Den gula linjen representerar en ökning av energi med multipler av antalet spinnkomponenter. **(b)** visar separationsenergin som funktion av partikelnummer, med optimerad interaktionsstyrka för att bäst följa experimentell data som svarta felmarginaler från [2]. Resultat med exakt diagonalisering från D'Amico och M. Rontani syns i grönt och de röda kryssen är våra beräknade resultat med andra ordningen störningsteori och samma interaktionsstyrka.

göra vinkelkorrektioner för varje mätning. Resultatet i 2D syns i figur 0.2b, och det lyckas tydligt återskapa de experimentella mätningarna i [3]. Utöver återskapandet av paulikristaller i 2D har vi utfört helt ny forskning som studerar hur interaktioner mellan partiklar påverkar paulikristaller i 1D och denna syns i 0.2c. Slutsaten är att repulsiva interaktioner gör att partiklarna befinner sig längre ifrån varandra och attraktiva att partiklar av olika spinn upplever en pareffekt i rummet där de dras mot varandra.

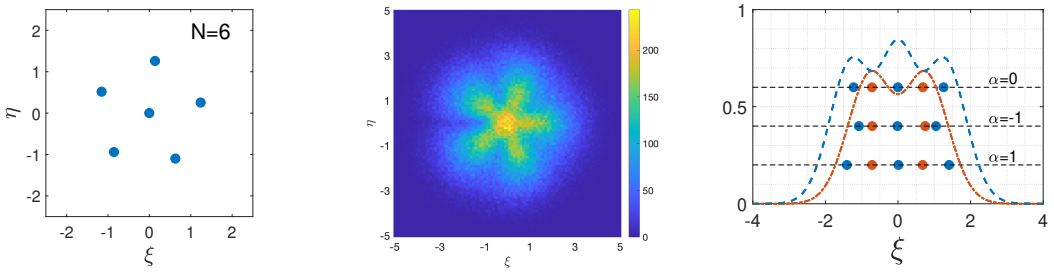

(a) **(b)** **(c)**

Figur 0.2: (a) visar sex partiklars mest sannolika konfiguration i den harmoniska potentialen, och (b) visar ett histogram över $5 \cdot 10^4$ masscentrum- och vinkelkorrigerade mätningar av sex partiklar. Paulikristallen för sex partiklar är synlig. (c) visar den mest sannolika positionen för fem partiklar för tre interaktionsstyrkor.

En intressant fortsättning på vår forskning hade varit att simulera paulikristaller med och utan störning i högre dimensioner, med fler partiklar, nya interaktionsmodeller eller till och med fermioniska molekyler [24].

Part II

Thesis

1
Background

In recent years, great advancements have been made in the field of quantum gases. A quantum gas is a system of particles where one cannot distinguish the particles based on their position, meaning that it is not possible to talk about *that* particle, but merely *a* particle [1]. These particles exhibit a universal behaviour, making it possible to model complicated systems by only studying the principles that govern a few particles. Quantum gases have become an intriguing field of research, where a small number of atoms are cooled and held in place for a short time by utilising the electrical field of a highly focused laser. Recent experiments in Zürn *et al.* [2] and Holten *et al.* [3] have studied specifically quantum gases consisting of a few ^{6}Li atoms in an optical trap. Their results showed clear patterns forming, such as pairing effects, magic numbers and Pauli crystals. This thesis aims to theoretically recreate these results by modelling the system as a few interacting fermions in a harmonic potential.

The following chapter is intended to give the reader an understanding of some essential concepts of quantum physics. We will go deeper into what constitutes a quantum gas, and concepts like fermions, bosons, and spin and their significance. Furthermore, we will go on to explain the general setup of an experiment with quantum gases and some basic mechanisms in play. Lastly we will mention what we want to achieve with this thesis, discuss how this knowledge can be applied to current matters and how research of quantum gases can contribute to our modern society.

1.1 Fermions, Bosons, and Spin

Everything in our known universe: energy, forces, and mass, can be divided into a smallest possible component. These components, or rather elementary particles, are then split into two categories: fermions like quarks and electrons, which constitute matter, and bosons like photons and gluons, which make up forces and energy. What determines this difference between bosons and fermions is a property called spin. It can be thought of as the quantum equivalent to angular momentum around a particle's own axis, although the particles are not actually spinning. Every species of elementary particle have a certain spin number that is either an integer, making it a boson, or a half-integer, making it a fermion [4]. A quantum gas can consist of either bosons, making it a Bose gas, or fermions, making it a Fermi gas. The latter is what will be studied in this thesis.

In the case of particles consisting of multiple elementary particles, the spin of its components is combined to form a total spin number [5]. An atom consisting of fermions like protons, neutrons and electrons can thus be regarded as either a boson, like ^{7}Li which has an integer total spin making it a composite boson, or a fermion, as in the case of ^{6}Li with its half-integer total spin making it a composite fermion. Furthermore, there are effects such as spin-orbit and spin-spin coupling that gives rise to fine and hyperfine corrections to the total angular momentum [4]. Two different hyperfine states of ^{6}Li were used in the modelled experiments [2], [3] and these will be treated as two different spin components σ, labelled up $\sigma = \uparrow$ and down $\sigma = \downarrow$ in the thesis.

The difference between composite fermions and bosons might seem insignificant at ordinary temperatures and pressures, where the two lithium atoms mentioned earlier exhibit very similar chemical properties. However, below a certain temperature quantum effects dominate and the

quantum nature of the atoms will emerge, showing some key differences [1]. This makes fermions, but not bosons, unable to occupy the same quantum state due to the Pauli exclusion principle.

The Pauli exclusion principle, or just the Pauli principle, states that two or more fermions in a system can not be in the same quantum state simultaneously [4]. Consequently, two fermions cannot occupy the same position in space. The Pauli principle is the driving factor for a number of effects such as the electron shell structure of atoms, Fermi gases, and Pauli crystals, where the latter will be studied extensively in chapter 5. The effect of the Pauli exclusion principle is especially evident in Fermi gases.

1.2 Quantum Gases

A quantum gas is a quantum-mechanical phase of matter that can be compared to an ideal classical gas, where the particles can move freely. However in contrast to classical gases, quantum gases exhibit a strict energy hierarchy and only exist at extremely high densities, like the conditions found in neutron stars, at least $10^{17}\,\mathrm{kg/m^3}$ [6], or extremely low temperatures at only a few nano-Kelvin. When a system of particles is cooled to temperatures close to absolute zero the speed of the particles, and therefore their momentum, becomes very small. As the momentum of the particles becomes less uncertain, Heisenberg's uncertainty principle claims that this makes the position of the particles more ambiguous. Consequently, the particles get "smeared out", which makes the de Broglie wavelength comparable to the interparticle distance. It is the latter that determines if the particles are considered to be a quantum gas, and if their behaviour is governed by quantum rules rather than classical physics. [1]

At these low temperatures Fermi gases and Bose gases exhibit very different behaviours. A Fermi gas will adhere to the Pauli principle and the particles will avoid being in the same positions, causing the gas to spread out. A Bose gas on the other hand is free from these constraints, which means that in theory all of the particles can occupy the same state. This will happen close to absolute zero and turn a Bose gas into a Bose-Einstein Condensate, which Carl Wieman, Eric Cornell, Wolfgang Ketterle were awarded the Nobel prize for in 2001. Since quantum gases are created in very controlled settings and the results can be generalised to more complicated systems due to the universal behaviour of the quantum particles, they are a exceptionally suited for experiments studying the effects of interactions and geometries.

1.3 Experimental Setup

Most experiments that study Fermi gases, such as [2], have similar experimental set ups, where they use a combination of an optical trap and a magneto-optical trap. Broadly speaking, an optical trap is when a highly focused laser is used to hold and move small particles. In the case of quantum gases, the electric field in the laser beam pulls the atoms towards the axis of the beam by inducing dipoles in the atoms. The electron density around the atom will always be higher at the end in the opposite direction of the electric field, and will therefore exert a force in that direction, while the positive pole of the atom will exert a force in the same direction as the field. Due to these opposing forces the atom will be slightly elongated. Since the forces of the electric field is strongest towards the middle of the beam, the pole of the atom closest to the beam axis will then exert the strongest force, thus dominating the direction of the movement of the atom. This results in a net inward force on the atom, keeping it in place. [1]

Before trapping the atoms in the single laser trap, they need to be cooled down in order to not just pass right through it, which they would do at room temperature. This is done with a magneto-optical trap and a phenomenon called "laser cooling". A magneto-optical trap consists of three perpendicular pairs of opposite facing lasers. The atoms are slowed down by utilising the Doppler effect and the fact that light has momentum. Since atoms moving towards a laser and away from the center of the trap will experience a blueshift, the laser wavelength is set to be slightly longer than the wavelength required for excitation. Then an atom moving against the laser

perceives the photon as slightly more energetic and will be able to absorb it. When an atom relaxes from an excited state, a photon is emitted in an arbitrary direction. On average, the atom is thus subject to a net force in the direction of the lasers, since it only absorbs photons from particular directions whereas emission occurs in all directions. Hence, the atoms are trapped and cooled. Lastly, the atoms are moved to the dipole trap and cooled to their final temperature by lowering the potential walls of the trap, simply letting redundant atoms evaporate through collision before restoring the trap. [1]

1.4 Applications

These experiments open up a world of potential applications, as a result of the universal behaviour of fermions. Firstly, it is possible to recreate the same patterns in Fermi gases that have been observed in atomic nuclei, where certain numbers of fermions have been noted to result in extra stable systems. These numbers are commonly referred to as magic numbers and are important within nuclear physics, as they are connected to the stability and decay of a nucleus [7]. Consequently, more research on magic numbers could for instance help us better understand heavier isotopes.

Secondly, experiments have shown that fermions in a Fermi gas tend to pair up in constellations known as Cooper pairs. This allows the fermions to form a sort of composite boson, and experience the phenomenon of superfluidity [5]. Superfluidity is when a fluid has zero viscosity and thus experiences no friction. For electrons, this is known specifically as superconductivity. Implementations of superfluidity has great value, as it allows paired fermions to move with an infinitesimal loss of energy, opening up possibilities of making more efficient energy systems. Consequently, modelling Fermi gases with pairing behaviour could lead to applications directed towards sustainable energy, as well as advancements within condensed matter physics. Furthermore, this pairing of fermions is also believed to exist in neutron stars. In neutron stars the density becomes so high that protons and electron fuse together forming neutrons, simultaneously as the Pauli principle of said neutrons prevents the star from imploding [6]. Consequently, by studying the Pauli principle and pairing in small controlled systems, it might be possible to construct models for systems such as neutron stars and superconductors.

1.5 Method and Delimitations

This project aims to model the behaviour of interacting Fermi gases consisting of a few particles trapped in a harmonic potential at temperatures near absolute zero. The purpose of this is to recreate the recent experimental work in [2] and [3], verifying the validity of our model. To achieve this, we firstly theoretically derive expressions for the non-interacting many-body wave function and its energies. Next, we add interactions between the particles and analytically derive the energy for two interacting particles. Because of the complexity of the analytical solution, we then treat the interaction as a perturbation for more than two particles and calculate the perturbed energy numerically. The results are compared with the experiments in [2] in chapter 4, where we find a pattern between the stability of the system and certain “magic” numbers of particles. Furthermore, we simulate Pauli crystals in chapter 5, comparing the results to [3], as well as conducting new research on the effect of interactions on Pauli crystals. The code used for simulations are numerical calculations are found in [8].

The thesis is restricted to primarily studying weakly interacting quantum gases with a few particles in one dimension, with the exception of Pauli crystals.

2

Theory and Analytical Derivations

In order to model multiple interacting particles in a trap we first need to understand the quantum mechanical description of non-interacting particles, and the confinement in which they reside. In the ultracold environment, atoms will be modelled as non-relativistic point particles with a trapping potential. This chapter will first introduce the single-particle wave function in a quantum harmonic oscillator and the corresponding Hamiltonian. Then, we study the many-body system by constructing the fermionic many-body wave function with a Slater determinant, introducing multiple spin components and calculating the energy of a non-interacting system. The non-interacting energy will form the basis for our own research in the next chapter, in which we calculate the energy for interacting systems.

2.1 The Single-Particle Wave Function

In contrast with classical physics where a particle can be described as confined to a point, a quantum particle is described as a wave spread out over all of coordinate space. The state of a single particle is represented by its wave function $\Psi(\vec{x}, t)$ [4]. Born's statistical interpretation says that $\left|\Psi(\vec{x}, t)\right|^2$ gives the probability of finding the particle at point $\vec{x}$ and time t. Upon observation, the wave function collapses to one measured state dictated by the probability density. The wave function is acquired by solving the Schrödinger equation

$$i\hbar\frac{\partial}{\partial t}\left|\Psi(t)\right\rangle = \hat{H}\left|\Psi(t)\right\rangle, \tag{2.1}$$

where $\hat{H}$ is the Hamiltonian of the system. In quantum mechanics, the wave function $\Psi(\vec{x}, t)$ is merely the coordinate representation of a general vector $\left|\Psi(t)\right\rangle$ residing in a Hilbert space and projected onto position space as $\Psi(\vec{x}, t) = \left\langle\vec{x}\middle|\Psi(t)\right\rangle$ [4]. A Hilbert space $\mathcal{H}$ is a vector space defined with the inner product

$$\langle f|g\rangle = \int_{\mathbb{R}^d} \mathrm{d}\vec{x}\, f^*(\vec{x})g(\vec{x}) < \infty, \tag{2.2}$$

where d is the number of dimensions in the system and $f, g \in \mathcal{H}$. $\left|\Psi(t)\right\rangle$ can be expanded in terms of a basis of eigenvectors $\{|\psi_n\rangle\}$ of a system's Hamiltonian $\hat{H}$ without losing any information. In coordinate space, the eigenstates are $\langle\vec{x}|\psi_n\rangle = \psi_n(\vec{x})$ and the wave function expanded using its eigenstates is

$$\Psi(\vec{x}, t) = \sum_n c_n\psi_n(\vec{x})e^{-\frac{iE_nt}{\hbar}}, \tag{2.3}$$

where $\sum_n |c_n|^2 = 1$ and $|c_n|^2$ is the probability of measuring the particle in a state $\psi_n(\vec{x})$. To obtain the eigenstates of a Hamiltonian, the stationary Schrödinger equation is solved

$$\hat{H}(\vec{x})\psi_n(\vec{x}) = E_n\psi_n(\vec{x}), \tag{2.4}$$

where E_n is the eigenenergy corresponding to the eigenvector $\psi_n(\vec{x})$. The eigenenergies are calculated with the help of the inner product and with the use of orthonormality between eigenstates, $\langle\psi_m|\psi_n\rangle = \delta_{mn}$, as

$$E_n = \langle\psi_n|\,\hat{H}\,|\psi_n\rangle = \int_{\mathbb{R}^d} \mathrm{d}\vec{x}\,\psi_n^*(\vec{x})\hat{H}\psi_n(\vec{x}). \tag{2.5}$$

2.2 The Quantum Harmonic Oscillator (QHO)

Having established the single particle wave function, we move on to the trapping potential where the particle resides and its Hamiltonian. A harmonic oscillator arises when the restoring force is linear, for example a spring obeying Hooke's law. Since the trap we model has a high intensity laser which keeps displacement from the focus small, we can make a first order Taylor series expansion. This is equivalent to assuming a linear restoring force, and thus a harmonic potential. The laser trap potential will therefore be modelled as a quantum harmonic oscillator (QHO). It is a favourable potential, being a quantum-mechanical system with an analytic solution to the Schrödinger equation. Furthermore, it is not difficult to generalise the QHO to multiple dimensions. In recent experiments [2], [9] a combination of the optical trapping methods described in 1.3 have been have been used to freeze out one and two dimensions respectively. Hence, it meaningful to create models that handle one, two and tree dimensions respectively.

The Hamiltonian for the one-dimensional QHO (1D-QHO) is written as

$$\hat{H}_{QHO}(x) = \frac{\hat{p}^2}{2m} + \frac{1}{2}m\omega^2\hat{x}^2 = -\frac{\hbar^2}{2m}\frac{d^2}{dx^2} + \frac{1}{2}m\omega^2 x^2. \tag{2.6}$$

where m is the particle mass, ω the characteristic angular frequency of the oscillator and x the position. The first term is the kinetic energy of the particle and the second term the surrounding potential $V(x)$. The n^{th} eigenstate $\psi_n(x) = \langle x|\psi_n\rangle$ is

$$\psi_n(x) = \frac{1}{\sqrt{2^n n!}}\left(\frac{m\omega}{\pi\hbar}\right)^{\frac{1}{4}} e^{-\frac{m\omega x^2}{2\hbar}} H_n\left(\sqrt{\frac{m\omega}{\hbar}}\, x\right), \tag{2.7}$$

with n being the principal quantum number and $H_n(x)$ the n^{th} Hermite polynomial. Using the characteristic length of the harmonic oscillator $l_{ho} = \sqrt{\hbar/m\omega}$, we can define the dimensionless coordinate $\xi = x/l_{ho}$. With this, equation (2.7) can be rewritten on dimensionless form as

$$\widetilde{\psi}_n(\xi) = \sqrt{l_{ho}}\cdot\psi_n(\xi) = \frac{1}{\sqrt{2^n n!}}\frac{1}{\pi^{\frac{1}{4}}} e^{-\frac{\xi^2}{2}} H_n(\xi), \tag{2.8}$$

satisfying

$$\int_{-\infty}^{\infty} \mathrm{d}\xi\, |\widetilde{\psi}_n(\xi)|^2 = 1, \tag{2.9}$$

which will be used in numerical calculations. The energy corresponding to the n^{th} eigenstate is $E_n = (n + \frac{1}{2})\hbar\omega$, where $\hbar\omega$ is the characteristic energy. An essential property in quantum mechanics is the "ground state", i.e. the state with the lowest energy. This is of interest because, according to the third law of thermodynamics, a system at zero temperature is in its ground state [10, p. 277-278]. The ground state of the 1D-QHO correspond to $n = 0$ with the energy $E_0 = \hbar\omega/2$. A visual representation of an occupied level, specifically the ground state of the one dimensional QHO is shown in figure 2.1.

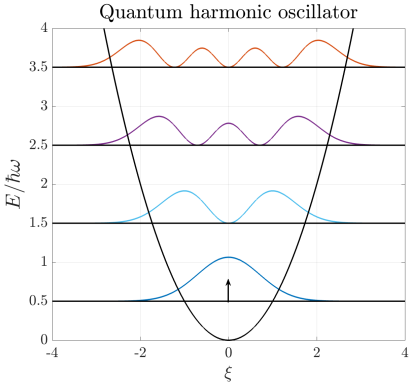

Figure 2.1: A visualisation of an occupied level of the 1D-QHO. The dimensionless characteristic energy is on the y-axis and the dimensionless length on the x-axis. Furthermore, $|\widetilde{\psi}_n(\xi)|^2$ of the first four quantum number and the potential $V(\xi) = \frac{1}{2}\xi^2$ are shown. The arrow ↑ indicates that the ground state $\widetilde{\psi}_0(\xi)$ is occupied.

In d dimensions, the quantum harmonic oscillator is separable into d one dimensional harmonic oscillators

$$\hat{H}_{QHO}(\vec{x}) = \sum_{i=1}^{d}\left(-\frac{\hbar^2}{2m}\frac{d^2}{dx_i^2} + \frac{1}{2}m\omega^2 x_i^2\right) = -\frac{\hbar^2}{2m}\nabla^2 + \frac{1}{2}m\omega^2|\vec{x}|^2. \tag{2.10}$$

Every harmonic oscillator will yield states with their own quantum numbers n_d and energies $E_{n,d}$, which can be added to form a quantum number $\vec{n}$ and energy E respectively. Specifically for

$d = 3$ we get $\vec{n} = (n_x, n_y, n_z)$ and $E_n = (n_x + n_y + n_z + \frac{3}{2})\hbar\omega$. This means that in higher dimensions, several states can correspond to the same energy eigenvalue, which is a phenomenon called degeneracy. Generally the degeneracy g_n is $1/2 \cdot (n+1)(n+2)$ in 3D and $(n+1)$ in 2D.

2.3 The Many-Body System

The single-particle system introduced now forms a foundation to build on as we move onto the many-body system. The Hamiltonian for many non-interacting particles is simply the sum of the single-particle Hamiltonians. Using equation (2.21), the Hamiltonian for N particles becomes

$$\hat{H} = \sum_{i=1}^{N} \left(-\frac{\hbar^2}{2m}\frac{\partial^2}{\partial x_i^2} + \frac{1}{2}m\omega^2 x_i^2 \right). \tag{2.11}$$

Observe that the many-particle case is identical to the many-dimension case, except that the subindex i denotes particle number, not dimensions and x_i is the position of the i^{th} particle. What the subindex refers to in a given situation will be made clear from context.

For N particles the many-body wave function is a product of single particle wave functions. In the case of two distinguishable particles in the two states ψ_a and ψ_b, the wave function can be expressed as $\psi(x_1, x_2) = \psi_a(x_1)\psi_b(x_2)$, called the Hartree product. However, fermions with the same spin are indistinguishable and antisymmetric under interchange, $\psi(x_1, x_2) = -\psi(x_2, x_1)$. They must therefore be described with a wave function that fulfills the antisymmetry criteria [4]. Thus, the normalised wave function for two fermions is

$$\Psi_{a,b}(x_1, x_2) = \frac{1}{\sqrt{2}}\big(\psi_a(x_1)\psi_b(x_2) - \psi_a(x_2)\psi_b(x_1)\big). \tag{2.12}$$

If two fermions are in the same state this wave function becomes zero, adhering to the Pauli exclusion principle. This many-body wave function can also be expressed as a determinant of a 2×2 matrix of all possible combinations of states and positions, which is called the Slater determinant for the system. A set of Slater determinants form a basis for the fermionic Fock space, which is the Hilbert space describing a quantum many body system with N indistinguishable particles. This is analogous to the single particle wave functions forming a basis for the Hilbert space. The scalar product that will be used in future calculations in the Fock space with N particles is defined as

$$\langle f|g\rangle = \prod_{l=1}^{N} \int_{-\infty}^{\infty} \mathrm{d}x_l \, f^*(x_l) g(x_l) < \infty. \tag{2.13}$$

2.3.1 The Slater Determinant

The Slater determinant is an algebraic construction which takes a many-body wave function and forces it to adhere to the Pauli principle. In chapter 5, the consequence of the Pauli principle on the wave function will be studied in more in detail. For N states and particles with the same spin it can be neatly written as a determinant of an $N \times N$ matrix with all the wave functions and coordinates:

$$\Psi_{n_1,\ldots,n_N}(x_1, x_2, \ldots, x_N) = \frac{1}{\sqrt{N!}} \begin{vmatrix} \psi_{n_1}(x_1) & \psi_{n_1}(x_2) & .... & \psi_{n_1}(x_N) \\ \psi_{n_2}(x_1) & \psi_{n_2}(x_2) & .... & \psi_{n_2}(x_N) \\ . & . & . & . \\ . & . & . & . \\ . & . & . & . \\ \psi_{n_N}(x_1) & \psi_{n_N}(x_2) & .... & \psi_{n_N}(x_N) \end{vmatrix}. \tag{2.14}$$

A normalisation constant $1/\sqrt{N!}$ is introduced, and as previously, ψ_{n_i} is a single particle state and n_i denotes an occupied state, for example $n_i = 0$ is the occupied ground state. A more compact way of expressing the Slater determinant that we will use in calculations is

$$\Psi_{n_1,...,n_N}(x_1, x_2, ..., x_N) = \frac{1}{\sqrt{N!}} \sum_{p \in S_N} \text{sign}(p) \left(\prod_{j=1}^{N} \psi_{n_{p(j)}}(x_j) \right). \tag{2.15}$$

S_N is the permutation group of N, containing all possible permutations p of N components. $\text{sign}(p) = \pm 1$ depending on if the permutation p is even or odd. Written explicitly the many-body wave function is a sum of all possible permutations of the states and positions of N particles. Occupied single particle 1D-QHO states in the many-particle case can neatly be visualised in figure 2.2.

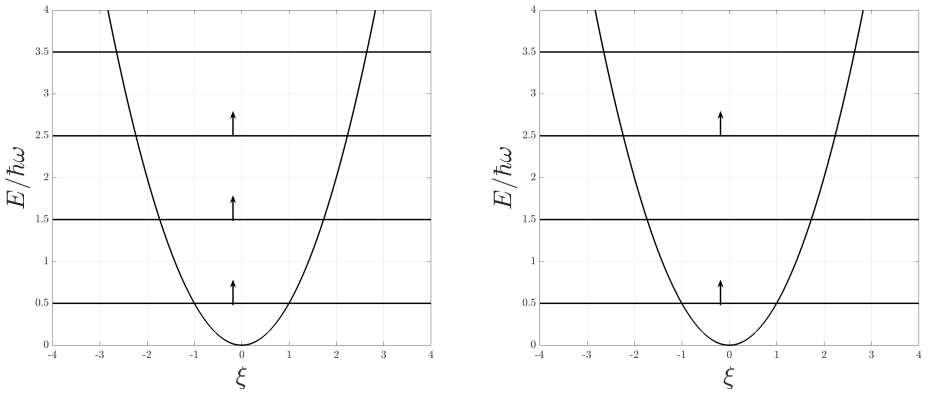

(a) First three 1D-QHO states occupied. **(b)** Two 1D-QHO states occupied.

Figure 2.2: Occupied 1D-QHO states for many particles visualised. The state three-particle state in **(a)** is a determinant of a 3×3 matrix and according to equation (2.14) the wave function would be $\Psi_{0,1,2}(x_1, x_2, x_3)$. Similarly, the two-particle state in **(b)** is a 2×2 Slater determinant with the wave function $\Psi_{0,2}(x_1, x_2)$. The state in **(a)** is the ground state for three particles and the state in **(b)** is an excited state for two particles.

The many-body wave functions constructed from the Slater determinant are orthonormal, which we prove by taking the inner product (2.13) of two wave functions $\Psi'_{n'_1 \ldots n'_N}$ and $\Psi_{n_1 \ldots n_N}$. Inserting equation 2.15 yields

$$\langle \Psi' | \Psi \rangle = \frac{1}{N!} \sum_{p' \in S_N} \text{sign}(p') \sum_{p \in S_N} \text{sign}(p) \prod_{l=1}^{N} \int \mathrm{d}x_l \; \psi^*_{n'_{p'(l)}}(x_l) \psi_{n_{p(l)}}(x_l). \tag{2.16}$$

The orthonormality of the single particle wave function $\{\psi_{n_i}(x_l)\}$ turns the integral into a product of Kronecker deltas $\delta_{n'_{p(l)} n_{p'(l)}}$, which is zero unless $p' = p$ and $n' = n$. Hence, the wave functions $\Psi' = \Psi$ must be equal for non-zero solutions and the result is

$$\langle \Psi' | \Psi \rangle = \langle \Psi | \Psi \rangle = \frac{1}{N!} \sum_{p \in S_N} \text{sign}^2(p) = \frac{1}{N!} \sum_{p \in S_N} 1 = \frac{1}{N!} \cdot N! = 1. \tag{2.17}$$

In summary, the inner product of two many-body wave functions is 1 if the wave functions represent the same state and 0 otherwise, proving the orthonormality. This result will be used in future calculations.

2.4 The Many-Body System: Multiple Spin Components

Everything up to this point has regarded systems with only one spin component, for example one hyperfine state of ^{6}Li. According to our interaction model that will be introduced properly in chapter 3, only particles of different spin interact, as we show in appendix A. Since our goal is to

study an interacting system, we consequently introduce the many-body wave function of multiple spin components and use it to calculate the energy in such a system. However, the interactions are not included in the calculation until the next chapter.

2.4.1 The Wave Function with Multiple Spin Components

For convenience the two spins in a two spin component ultracold Fermi gas will be denoted with spin up ($\sigma = \uparrow$) and spin down ($\sigma = \downarrow$). These are not necessarily the spin up and down states of an electron as the spin values are not important for the calculations; they could for example be the two hyperfine states of lithium used in [2] and [3]. The total number of particles is $N = N_\uparrow + N_\downarrow$, where $N_\uparrow$ is the number of particles in the spin up state and $N_\downarrow$ the number of particles in the spin down state. Due to particles of different spin being distinguishable, the wave function with two spin components is given by the Hartree product of the two spin states

$$\begin{aligned}\Psi_{n_{\uparrow 1},...,n_{\uparrow N_\uparrow},n_{\downarrow 1},...,n_{\downarrow N_\downarrow}}(x_{\uparrow 1},...,x_{\uparrow N_\uparrow},x_{\downarrow 1},...,x_{\downarrow N_\downarrow}) \\ = {}^{\uparrow}\Psi_{n_{\uparrow 1},...,n_{\uparrow N_\uparrow}}(x_{\uparrow 1},...,x_{\uparrow N_\uparrow}) \cdot {}^{\downarrow}\Psi_{n_{\downarrow 1},...,n_{\downarrow N_\downarrow}}(x_{\downarrow 1},...,x_{\downarrow N_\downarrow}),\end{aligned} \tag{2.18}$$

where $x_{\sigma i}$ is the coordinate of the i^{th} particle with spin σ and $n_{\sigma i}$ is the i^{th} state for a particle with spin σ. Note that the left subindex always indicates what spin a particle is in and the right subindex counts particles. This can be generalised to multiple spin components and written compactly as

$$\Psi = \prod_\sigma {}^{\sigma}\Psi_{n_{\sigma 1},...,n_{\sigma N_\sigma}}(x_{\sigma 1},...,x_{\sigma N_\sigma}), \tag{2.19}$$

where the total number of particles is $N = \sum_\sigma N_\sigma$. Furthermore, the wave function ${}^{\sigma}\Psi$ is given by (2.14) as

$${}^{\sigma}\Psi_{n_{\sigma 1}...n_{\sigma N_\sigma}}(x_{\sigma 1},...,x_{\sigma N_\sigma}) = \frac{1}{\sqrt{N_\sigma!}} \sum_{p \in S_{N_\sigma}} \text{sign}(p) \left(\prod_{i=1}^{N_\sigma} \psi_{n_{\sigma p(i)}}(x_{\sigma i}) \right) \tag{2.20}$$

The orthonormality of the many-body wave function with many spin components is shown by applying equation (2.17). Furthermore, an important property of a many spin component system is that every 1D-QHO energy level can now hold up to one particle of each spin component.

2.4.2 The Energy of an Eigenstate with Multiple Spin Components

To study the correlation between certain particle numbers and stability, we must calculate the eigenenergies of a many-body system. The Hamiltonian without interactions between particles of a two spin component system is a sum of the Hamiltonian of each spin component

$$\hat{H} = \sum_{i=1}^{N_\uparrow} \hat{H}_{QHO}(x_{\uparrow i}) + \sum_{j=1}^{N_\downarrow} \hat{H}_{QHO}(x_{\downarrow j}) = {}^{\uparrow}\hat{H} + {}^{\downarrow}\hat{H}. \tag{2.21}$$

To solve the stationary Schrödinger equation $\hat{H}\Psi = E\Psi$ and obtain the eigenenergy of a many-body eigenstate, we use the eigenvalue problem of single-particle wave functions. Inserting the single particle Hamiltonian $\hat{H}_{QHO}(x)$ into the stationary Schrödinger equation

$$\hat{H}_{QHO}(x)\psi_{n_i}(x) = \varepsilon_{n_i}\psi_{n_i}(x), \tag{2.22}$$

gives the single particle energies $\varepsilon_{n_i} = \hbar\omega\left(n_i + \frac{1}{2}\right)$. Because the wave function Ψ is a product of two single spin wave functions, separation of variables is applicable. Consequently, we can solve the eigenvalue problems ${}^{\uparrow}\hat{H}{}^{\uparrow}\Psi = {}^{\uparrow}E{}^{\uparrow}\Psi$ and ${}^{\downarrow}\hat{H}{}^{\downarrow}\Psi = {}^{\downarrow}E{}^{\downarrow}\Psi$ separately and gain the total energy

$E = {}^{\uparrow}E + {}^{\downarrow}E$. Equation (2.22) gives the eigenvalue of ${}^{\uparrow}\hat{H}{}^{\uparrow}\Psi$ as

$$\begin{aligned} {}^{\uparrow}\hat{H}{}^{\uparrow}\Psi &= \frac{1}{\sqrt{N_{\uparrow}!}} \sum_{p \in S_{N_{\uparrow}}} \operatorname{sign}(p) \sum_{i=1}^{N_{\uparrow}} \hat{H}_{QHO}(x_{\uparrow i}) \left(\prod_{j=1}^{N_{\uparrow}} \psi_{n_{\uparrow p(j)}} \left(x_{\uparrow j} \right) \right) \\ &= \frac{1}{\sqrt{N_{\uparrow}!}} \sum_{p \in S_{N_{\uparrow}}} \operatorname{sign}(p) \left(\sum_{i=1}^{N_{\uparrow}} \varepsilon_{n_{\uparrow p(i)}} \right) \prod_{j}^{N_{\uparrow}} \psi_{n_{\uparrow p(j)}} \left(x_{\uparrow j} \right) = \left(\sum_{i=1}^{N_{\uparrow}} \varepsilon_{\uparrow i} \right) {}^{\uparrow}\Psi. \end{aligned} \tag{2.23}$$

The calculation is identical for the spin down case. The total eigenvalue of the Hamiltonian is thus

$$\hat{H}\Psi = \left(\sum_{i=1}^{N_{\uparrow}} \varepsilon_{\uparrow i} + \sum_{j=1}^{N_{\downarrow}} \varepsilon_{\downarrow j} \right) \Psi \tag{2.24}$$

with the eigenenergy

$$E = \hbar\omega \left(\frac{N}{2} + \sum_{i=1}^{N_{\uparrow}} n_{\uparrow i} + \sum_{j=1}^{N_{\downarrow}} n_{\downarrow j} \right) \tag{2.25}$$

The important conclusion to be drawn from (2.25) is that without any interaction between particles of different spin, the energy of a many-body wave function is the sum of energies of occupied single-particle states. Generalising the calculations to multiple spin components gives

$$\hat{H} = \sum_{\sigma} {}^{\sigma}\hat{H} \text{ and } E = \sum_{\sigma} E_{\sigma}, \tag{2.26}$$

with the total eigenenergy written explicitly as

$$E = \hbar\omega \left(\frac{N}{2} + \sum_{\sigma} \sum_{i=1}^{N_{\sigma}} n_{\sigma i} \right), \text{ if } \Psi' = \Psi, \text{ else } 0. \tag{2.27}$$

3

Interacting Many-Body System

Since realistic interactions between particles are rather complicated, it is commonplace to use a shape-independent approximation consisting of an interaction potential with zero range. Hence, a delta function will be used to model the interaction between particles. This is an appropriate approximation because at ultracold temperatures, the de Broglie wavelength h/p [1] will be large enough for the wave functions of particles to overlap, hence render the finer details of the interaction potential irrelevant [11]. The total Hamiltonian for our model for two spins thus becomes

$$\hat{H} = \sum_{i=1}^{N_\uparrow} \hat{H}_{QHO}(x_{\uparrow i}) + \sum_{j=1}^{N_\downarrow} \hat{H}_{QHO}(x_{\downarrow j}) + \sum_{i=1}^{N_\uparrow}\sum_{j=1}^{N_\downarrow} \alpha\delta(x_{\uparrow i} - x_{\downarrow j}), \tag{3.1}$$

where the interaction term only involves particles of different spin. A verification of the model where only particles of different spin interact is found in appendix A. The interaction strength α is possible to tune experimentally using an external magnetic field by a mechanism called Feshbach resonance, provided the atoms are in an ultracold environment [12].

In this chapter we will first derive an analytical expression for the energy of two interacting particles. Due to the complexity of the analytical solutions for more than two particles, we will then transition to treating the interactions as a perturbation and use perturbation theory to calculate the energy of the interacting system for one and multiple spin components. From there, we can start modelling experiments in the next chapter, finding magic numbers and pairing effects.

3.1 Analytical Solution of Two Interacting Particles in 1D

As previously mentioned, the Schrödinger equation for two particles with two different spin can be solved analytically with $N_\uparrow = N_\downarrow = 1$. The problem already have a known solution, which was derived by Busch *et al.* for two fermions in three dimensions in [11]. We calculate the one-dimensional case. The solution is our own original work, and the full, detailed solution is available in appendix C.

To start off, the Hamiltonian for the two-particle system can be written as the sum of two single-particle Hamiltonians and an interaction potential

$$\hat{H} = -\frac{\hbar^2}{2m}\frac{\partial^2}{\partial x_1^2} - \frac{\hbar^2}{2m}\frac{\partial^2}{\partial x_2^2} + V_{pot}(x_1) + V_{pot}(x_2) + V_{int}(x_1 - x_2), \tag{3.2}$$

where $V_{pot}(x) = m\omega^2 x^2/2$ and $V_{int}(x) = \alpha\delta(x)$. This Hamiltonian can be split into two parts by defining two new coordinates, $R = (x_1 + x_2)/2$ and $r = (x_1 - x_2)$, which are a centre-of-mass coordinate and a relative coordinate, respectively. We can thereby split the Hamiltonian into a

[1] The most probable velocity of a particle in thermal equilibrium with its environment is given by the Maxwell–Boltzmann distribution as $v = \sqrt{2k_BT/m}$. For an ultracold ($\sim$ µK) ^{6}Li atom $h/p \approx 10^4$ Å, while a typical atom is ~ 1 Å across.

centre-of-mass part and a relative part:

$$\begin{aligned}\hat{H}_{CoM}(R) &= -\frac{\hbar^2}{2M}\frac{\partial^2}{\partial R^2} + \frac{1}{2}M\omega^2 R^2, \\ \hat{H}_{rel}(r) &= -\frac{\hbar^2}{2\mu}\frac{\partial^2}{\partial r^2} + \frac{1}{2}\mu\omega^2 r^2 + \alpha\delta(r).\end{aligned} \tag{3.3}$$

$M = 2m$ is the total mass and $\mu = m/2$ is the reduced mass. The centre of mass part, $\hat{H}_{CoM}$, is just a harmonic oscillator with eigenenergies $\hbar\omega(n + 1/2)$, while the relative part, $\hat{H}_{rel}$, looks like a one-dimensional QHO with a delta function potential at the origin. We focus on solving the relative part. To continue, we define a new harmonic oscillator length for the relative equation as

$$\lambda_{ho} = \sqrt{\frac{\hbar}{\mu\omega}} = \sqrt{2}\, l_{ho}, \tag{3.4}$$

where l_{ho} is the standard harmonic oscillator length. The Hamiltonian is turned into its dimensionless form

$$\hat{H}_r(\xi) = -\frac{1}{2}\frac{\partial^2}{\partial\xi^2} + \frac{1}{2}\xi^2 + \frac{\alpha}{\hbar\omega\lambda_{ho}}\delta(\xi) = -\frac{1}{2}\frac{\partial^2}{\partial\xi^2} + \frac{1}{2}\xi^2 + \frac{\beta}{\sqrt{2}}\delta(\xi) \tag{3.5}$$

and β is defined as

$$\beta = \frac{\sqrt{2}\,\alpha}{\hbar\omega\lambda_{ho}} = \frac{\alpha}{\hbar\omega l_{ho}}. \tag{3.6}$$

We insert the new dimensionless Hamiltonian $\hat{H}_r$ into the the stationary Schrödinger equation $\hat{H}_r\Psi(\xi) = E\Psi(\xi)$, where E is the eigenenergy for the relative Hamiltonian. To solve the Schrödinger equation we expand $\Psi(\xi)$ in the basis of the free single particle wave functions, $\psi_n(x)$, with the expansion coefficents c_n. Then, we calculate c_n by projecting on $\psi_n^*(x)$ and insert the 1D-QHO energies E_n. By simplifying the resulting expression we get

$$-\frac{1}{\beta} = \frac{1}{\sqrt{2}}\sum_m \frac{\psi_m^*(0)\psi_m(0)}{E_m - E} = \frac{1}{\sqrt{2}}\sum_m \frac{|\psi_m(0)|^2}{E_m - E}. \tag{3.7}$$

To continue and gain an explicit correlation between the interaction strength and energy we need to evaluate the sum. As $\hat{H}_{QHO}$ is a normal harmonic oscillator, its wave functions $\widetilde{\psi}_m(\xi)$ are known from equation (2.8), where we replace $\widetilde{\psi}_m(\xi)$ with $\psi_m(\xi)$ for simpler notation. For odd m, the wave function at $\xi = 0$ becomes zero due to the Hermite polynomial and the solution becomes trivial. The physical interpretation of this would be that states with an odd relative wave function cannot interact through the delta potential V_{int}. To eliminate the redundant parts, we use the variable substitution $m = 2n$. Inserting ψ_{2n} and E_{2n} into one term of the sum from equation (3.7), we get

$$\frac{1}{\sqrt{2}}\frac{|\psi_{2n}(0)|^2}{E_{2n} - E} = \frac{1}{\sqrt{2\pi}}\frac{(H_{2n}(0))^2}{(2^{2n}(2n)!)(2n + \frac{1}{2} - E)} = \frac{1}{2\sqrt{2\pi}}\frac{1}{2^{2n}}\frac{\frac{(H_{2n}(0))^2}{(2n)!}}{n - (\frac{E}{2} - \frac{1}{4})}. \tag{3.8}$$

From here, an integral substitution allows us to use the generating function for the squared Hermite polynomials [13, p. 250] to get rid of any n-dependence, which means we can write equation (3.7), the entire sum, as

$$-\frac{1}{\beta} = \frac{1}{2\sqrt{2\pi}}\int_0^\infty \mathrm{d}x (x)^{-\nu-1}\,(1+x)^{-1/2+\nu}\,, \tag{3.9}$$

where $\nu = \left(\frac{E}{2} - \frac{1}{4}\right)$. The integral looks like the integral representation of Tricomi's confluent hypergeometric function [14, p. 505], which allows us to exchange the integral. Finally, the properties of this confluent hypergeometric function allows us to attain an expression for $\beta(E)$, linking the relative energy between the particles and the interaction strength:

$$\beta(E) = -2\sqrt{2}\frac{\Gamma\left(-\frac{E}{2} + \frac{3}{4}\right)}{\Gamma\left(-\frac{E}{2} + \frac{1}{4}\right)}. \tag{3.10}$$

By inverting this function numerically, we can find the energy as a function of interaction strength, $E(\beta) = E(\alpha/l_{ho}\hbar\omega)$. In figure 3.1 we see the function $E(\alpha/l_{ho}\hbar\omega)$. Its asymptotic behaviour occurs due to the gamma function diverging for negative integer inputs. The branches of the function can be interpreted as belonging to different states of the relative part with some quantum number k; we write the energy as $E_k(\alpha/l_{ho}\hbar\omega)$ to clarify this. Note that $E_k(0)$ corresponds to the energies $\hbar\omega(1/2+2k)$. This function completely models the energy of the relative part of the Hamiltonian, while the energy for the centre-of-mass part is simply $\hbar\omega(n+\frac{1}{2})$, for some quantum number n. Thus, the energy for the entire system is

$$E_{\text{total}}(n,k,\alpha) = \frac{\hbar\omega}{2} + n\hbar\omega + E_k\left(\frac{\alpha}{l_{ho}\hbar\omega}\right). \tag{3.11}$$

The process for analytically calculating the interaction between particles is very difficult and time consuming, even only considering two particles. Needless to say, extending this solution to many particles of different spins would be practically impossible. Clearly, an approximate solution like perturbation theory is necessary.

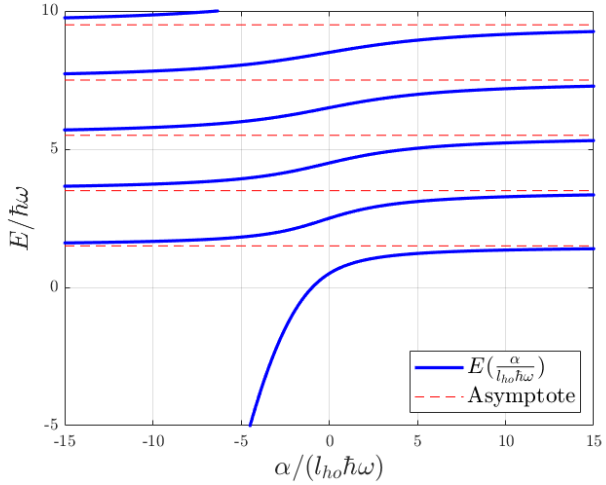

Figure 3.1: A plot of the implicitly derived function $E(\beta) = E(\alpha/l_{ho}\hbar\omega)$.

3.2 Time-independent Perturbation Theory

Perturbation theory is a procedure to approximating solutions of the Schrödinger equation for a potential with an already known solution that is slightly perturbed. This is achieved by calculating the order of corrections to the eigenenergies E_n and eigenstates Ψ_n. This section will introduce the theory behind non-degenerate perturbation theory as it is presented in [4] and the following sections will implement it on interacting systems.

The unperturbed system satisfies the time-independent Schrödinger equation $\hat{H}^{(0)}\Psi_n^{(0)} = E_n^{(0)}\Psi_n^{(0)}$. Adding the perturbation $\alpha\hat{H}'$, where α is of small amplitude, results in

$$\hat{H} = \hat{H}^{(0)} + \alpha\hat{H}' \tag{3.12}$$

$$\Psi_n = \Psi_n^{(0)} + \alpha\Psi_n^{(1)} + \alpha^2\Psi_n^{(2)}\ldots \tag{3.13}$$

$$E_n = E_n^{(0)} + \alpha E_n^{(1)} + \alpha^2 E_n^{(2)}\ldots \tag{3.14}$$

where $E_n^{(k)}$ and $\Psi_n^{(k)}$ is the k^{th} order correction to energy, respectively energy eigenstate. Up to first order in α, the first order energy correction is given by

$$E_n^{(1)} = \left\langle \Psi_n^{(0)} \middle| H' \middle| \Psi_n^{(0)} \right\rangle, \tag{3.15}$$

and the energy eigenstate correction

$$\Psi_n^{(1)} = \sum_{n \neq m} \frac{\left\langle \Psi_m^{(0)} \right| H' \left| \Psi_n^{(0)} \right\rangle}{E_n^{(0)} - E_m^{(0)}} \Psi_m^{(0)}. \tag{3.16}$$

Up to second order in α, the expression of the second order energy correction is

$$E_n^{(2)} = \sum_{m \neq n} \frac{\left| \left\langle \Psi_n^{(0)} \right| H' \left| \Psi_m^{(0)} \right\rangle \right|^2}{E_n^{(0)} - E_m^{(0)}}. \tag{3.17}$$

3.3 Interaction in a Two-Component System

Having introduced perturbation theory, we can derive expressions for the eigenenergies of an interacting system with two spin components. This will later be compared to the experiments in [2]. The interaction, where only particles of different spin interact, is written as

$$\hat{H}' = \sum_{i=1}^{N_\uparrow} \sum_{j=1}^{N_\downarrow} \delta(x_{\uparrow i} - x_{\downarrow j}). \tag{3.18}$$

In appendix A it is shown that particles of the same spin do not interact through a delta potential. This interaction will be treated as a perturbation and to calculate the corrections from the previous section, we need to evaluate $\langle \Psi | \hat{H}' | \Psi' \rangle$, called the overlap integral. We will look at the general case with an overlap integral between different states Ψ and Ψ', where the first order energy correction $E^{(1)}$ is attained with $\Psi = \Psi'$. The case $\Psi \neq \Psi'$ is relevant when calculating the perturbed eigenstate in (3.16) and the second order energy correction in (3.17). Inserting the compact Slater determinants into the overlap integral and simplifying gives

$$\begin{aligned}
\langle \Psi | \hat{H}' | \Psi' \rangle = & \frac{1}{N_\uparrow! N_\downarrow!} \sum_{p,p' \in S_{N_\uparrow}} \operatorname{sign}(p) \operatorname{sign}(p') \sum_{\tilde{p},\tilde{p}' \in S_{N_\downarrow}} \operatorname{sign}(\tilde{p}) \operatorname{sign}(\tilde{p}') \\
& \times \sum_{i=1}^{N_\uparrow} \sum_{j=1}^{N_\downarrow} \int \mathrm{d}x_{\uparrow i}\, \mathrm{d}x_{\downarrow j}\, \psi^*_{n_{p(i)}}(x_{\uparrow i}) \psi^*_{n_{\tilde{p}(j)}}(x_{\downarrow j}) \delta(x_{\uparrow i} - x_{\downarrow j}) \psi_{n'_{p'(i)}}(x_{\uparrow i}) \psi_{n'_{\tilde{p}'(j)}}(x_{\downarrow j}) \\
& \times \prod_{l \neq i} \int \mathrm{d}x_{\uparrow l}\, \psi^*_{n_{p(l)}}(x_{\uparrow l}) \psi_{n'_{p'(l)}}(x_{\uparrow l}) \prod_{k \neq j} \int \mathrm{d}x_{\downarrow k}\, \psi^*_{n_{\tilde{p}(k)}}(x_{\downarrow k}) \psi_{n'_{\tilde{p}'(k)}}(x_{\downarrow k}).
\end{aligned} \tag{3.19}$$

The delta function acts on the second line, while the orthonormality of the single particle wave function turns the third line into Kronecker deltas, yielding the expression

$$\begin{aligned}
\langle \Psi | \hat{H}' | \Psi' \rangle = & \frac{1}{N_\uparrow! N_\downarrow!} \sum_{p,p' \in S_{N_\uparrow}} \operatorname{sign}(p) \operatorname{sign}(p') \sum_{\tilde{p},\tilde{p}' \in S_{N_\downarrow}} \operatorname{sign}(\tilde{p}) \operatorname{sign}(\tilde{p}') \\
& \times \sum_{i=1}^{N_\uparrow} \sum_{j=1}^{N_\downarrow} \int \mathrm{d}x_{\downarrow j}\, \psi^*_{n_{p(i)}}(x_{\downarrow j}) \psi^*_{n_{\tilde{p}(j)}}(x_{\downarrow j}) \psi_{n'_{p'(i)}}(x_{\downarrow j}) \psi_{n'_{\tilde{p}'(j)}}(x_{\downarrow j}) \\
& \times \prod_{l \neq i} \delta_{n_{p(l)} n'_{p'(l)}} \prod_{k \neq j} \delta_{n_{\tilde{p}(k)} n'_{\tilde{p}'(k)}}.
\end{aligned} \tag{3.20}$$

This expression sets limitations on the quantum numbers and by varying them we get all the different cases for the overlap integral. Fortunately, most cases can be excluded immediately. Firstly, if ${}^\sigma\Psi$ and ${}^\sigma\Psi'$ have two or more particles occupying different single particle states, the Kronecker deltas make $\langle \Psi | \hat{H}' | \Psi' \rangle = 0$. Furthermore, the expression is also zero if the states have

different numbers of particles. The remaining cases have the restriction that $n_{p(l)} = n'_{p'(l)}$ and $n_{\tilde{p}(k)} = n'_{\tilde{p}'(k)}$ due to the Kronecker deltas, and are therefore only dependent on the remaining quantum numbers $n_{p(i)}$, $n'_{p'(i)}$, $n_{\tilde{p}(j)}$, and $n'_{\tilde{p}'(j)}$. The four possible cases are

$$\begin{aligned} &\text{Case 1: } n_{p(i)} = n'_{p'(i)} \text{ and } n_{\tilde{p}(j)} = n'_{\tilde{p}'(j)}, \\ &\text{Case 2: } n_{p(i)} \neq n'_{p'(i)} \text{ and } n_{\tilde{p}(j)} = n'_{\tilde{p}'(j)}, \\ &\text{Case 3: } n_{p(i)} = n'_{p'(i)} \text{ and } n_{\tilde{p}(j)} \neq n'_{\tilde{p}'(j)}, \\ &\text{Case 4: } n_{p(i)} \neq n'_{p'(i)} \text{ and } n_{\tilde{p}(j)} \neq n'_{\tilde{p}'(j)}. \end{aligned} \tag{3.21}$$

Case 1: This is equivalent with $\Psi = \Psi'$. Consequently, the overlap integral becomes the expression of the first order energy correction according to equation (3.15). Since $p = p'$ and $\tilde{p} = \tilde{p}'$, the first row in equation (3.20) is simply 1. By using this simplification and by inserting the dimensionless wave function, the overlap integral for the first case becomes

$$E^{(1)} = \langle \Psi | \, \hat{H}' \, | \Psi \rangle = \frac{1}{l_{ho}} \sum_{i=1}^{N_\uparrow} \sum_{j=1}^{N_\downarrow} \int \mathrm{d}\xi \, |\widetilde{\psi}_{n_i}(\xi)|^2 |\widetilde{\psi}_{n_j}(\xi)|^2. \tag{3.22}$$

Case 2: For the inequality we simplify the expression by setting $n_{p(i)} = n_\kappa$ and $n'_{p'(i)} = n'_\lambda$, with $n_\kappa \neq n'_\lambda$. The equality implies the equivalence $n_{\tilde{p}(j)} = n'_{\tilde{p}'(j)} \Leftrightarrow \tilde{p} = \tilde{p}' \Leftrightarrow {}^\downarrow\Psi = {}^\downarrow\Psi'$. Thus the spin down states are the same, while the spin up states differ with one particle. This can be visualised in figure 3.2 for the particular case of $N_\uparrow = N_\downarrow = 3$. Referring to the visual representation of occupied single particle state, Ψ could be represented by figure 3.2a and Ψ' by figure 3.2b.

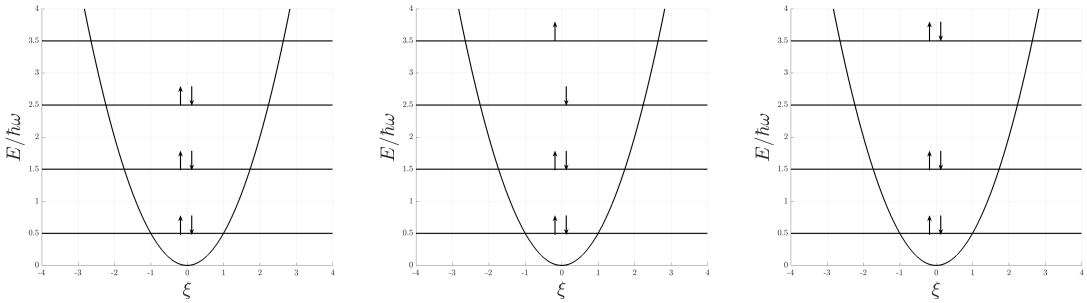

(a) **(b)** **(c)**

Figure 3.2: Three different occupied states for $N = 6$ with $N_\uparrow = 3$ and $N_\downarrow = 3$. Each energy level can be twice occupied, once by $\sigma = \uparrow$ and once by $\sigma = \downarrow$.

Using the conclusions from above and repeating similar steps as for case one, shown explicitly in equation (B.1), the overlap integral becomes

$$\langle \Psi | \hat{H}' | \Psi' \rangle = \frac{1}{l_{ho}} \sum_{j=1}^{N_\downarrow} \int \mathrm{d}\xi \, \widetilde{\psi}^*_{n_\kappa}(\xi) \widetilde{\psi}_{n'_\lambda}(\xi) |\widetilde{\psi}_{n_j}(\xi)|^2. \tag{3.23}$$

Case 3: This is very similar to the second case. The equality in equation (3.21) implies the equivalence $n_{p(i)} = n'_{p'(i)} \Leftrightarrow p = p' \Leftrightarrow {}^\uparrow\Psi = {}^\uparrow\Psi'$, meaning that the occupied spin up levels are the same, while the occupied spin down levels differ with one particle. This case can be visualised in figure 3.2, where Ψ could be represented by 3.2b and Ψ' by figure 3.2c. We denote the quantum numbers that differ by $n_{\tilde{p}(j)} = n_\mu$ and $n'_{\tilde{p}'(j)} = n'_\nu$, and similarly to case two, $n_\mu \neq n'_\nu$. The overlap integral in case three is derived in exactly the same manner as case two but instead of the sum in (3.23) running over all occupied spin down levels, case three runs over all occupied spin up levels:

$$\langle \Psi | \hat{H}' | \Psi' \rangle = \frac{1}{l_{ho}} \sum_{i=1}^{N_\uparrow} \int \mathrm{d}\xi \, \widetilde{\psi}^*_{n_\mu}(\xi) \widetilde{\psi}_{n'_\nu}(\xi) |\widetilde{\psi}_{n_i}(\xi)|^2. \tag{3.24}$$

Case 4: This means that the states ${}^{\sigma}\Psi$ and ${}^{\sigma}\Psi'$ differ by one occupied level and can be visualised in figure 3.2, where Ψ could be represented by 3.2a and Ψ' by 3.2c. Referring to equation (3.21), we set $n_{p(i)} = n_\kappa$ and $n'_{p'(i)} = n'_\lambda$, with $n_\kappa \neq n'_\lambda$, as well as $n_{\tilde{p}(j)} = n_\mu$ and $n'_{\tilde{p}'(j)} = n'_\nu$, with $n_\mu \neq n'_\nu$. With similar derivation to the previous cases, shown explicitly in equation (B.2), the overlap integral becomes

$$\langle \Psi | \hat{H}' | \Psi' \rangle = \frac{1}{l_{ho}} \int \mathrm{d}\xi \, \widetilde{\psi}^*_{n_\kappa}(\xi) \widetilde{\psi}^*_{n'_\mu}(\xi) \widetilde{\psi}_{n_\lambda}(\xi) \widetilde{\psi}_{n'_\nu}(\xi). \tag{3.25}$$

For the second order energy perturbation approximation, equation (3.17) indicates that we must calculate a sum over many different overlap integrals. However, we have now shown that there are only five different cases for how these overlap integrals may look, and consequently, these are found in table 3.1.

Cases	$\langle \Psi \lvert \hat{H}' \rvert \Psi' \rangle$	Example state in Fig. 3.2 **(a)**	**(b)**	**(c)**
Case 1:	$\frac{1}{l_{ho}} \sum_{i=1}^{N_\uparrow} \sum_{j=1}^{N_\downarrow} \int \mathrm{d}\xi \, \lvert\widetilde{\psi}_{n_i}(\xi)\rvert^2 \lvert\widetilde{\psi}_{n_j}(\xi)\rvert^2$	$\Psi = \Psi'$		
Case 2:	$\frac{1}{l_{ho}} \sum_{j=1}^{N_\downarrow} \int \mathrm{d}\xi \, \widetilde{\psi}^*_{n_\kappa}(\xi) \widetilde{\psi}_{n'_\lambda}(\xi) \lvert\widetilde{\psi}_{n_j}(\xi)\rvert^2$	Ψ	Ψ'	-
Case 3:	$\frac{1}{l_{ho}} \sum_{i=1}^{N_\uparrow} \int \mathrm{d}\xi \, \widetilde{\psi}^*_{n_\mu}(\xi) \widetilde{\psi}_{n'_\nu}(\xi) \lvert\widetilde{\psi}_{n_i}(\xi)\rvert^2$	-	Ψ	Ψ'
Case 4:	$\frac{1}{l_{ho}} \int \mathrm{d}\xi \, \widetilde{\psi}^*_{n_\kappa}(\xi) \widetilde{\psi}^*_{n'_\mu}(\xi) \widetilde{\psi}_{n_\lambda}(\xi) \widetilde{\psi}_{n'_\nu}(\xi)$	Ψ	-	Ψ'
Else:	0	-		

Table 3.1: The overlap integral for the five different cases. The right column refer to which figure in 3.2 the states Ψ and Ψ' could correspond to. The last case, labelled else, applies when ${}^{\sigma}\Psi$ and ${}^{\sigma}\Psi'$ occupy two or more different levels, or if they have different particle numbers.

Conclusively, most terms in the sum for the second order correction will be zero, which greatly simplifies calculations. Interpreting the results further, we observe that the magnitude of the interaction depends directly on how much the wave functions overlap. In the following chapter, these overlap integrals will be evaluated numerically and compared to the experimental results in [2] by using both first and second order perturbation theory.

3.4 Interaction in a Multiple Spin Component System

Before the results are compared, we generalise the conclusions to multiple spin components. Assuming pairwise interaction between particles, the perturbation describing the interaction between particles becomes

$$\hat{H}' = \sum_{\sigma \neq \sigma'} \left(\sum_{i=1}^{N_\sigma} \sum_{j=1}^{N_{\sigma'}} \delta(x_{\sigma i} - x_{\sigma' j}) \right), \tag{3.26}$$

where only particles of different spin interact, in accordance with equation (A.4). The derivation of the first order energy correction to the unperturbed system is identical to equation (3.22), except for the additional use of the orthonormality of the many-body wave function (2.17), yielding

$$E^{(1)} = \sum_{\sigma \neq \sigma'} \left(\sum_{i=1}^{N_\sigma} \sum_{j=1}^{N_{\sigma'}} \frac{1}{l_{ho}} \int d\xi \lvert\widetilde{\psi}_{n_{\sigma i}}(\xi)\rvert^2 \lvert\widetilde{\psi}_{n_{\sigma' j}}(\xi)\rvert^2 \right). \tag{3.27}$$

4

Numerical Results

In the previous chapter, necessary expressions for computing interactions with perturbation theory were derived. Here, we present our results for the energy of an interacting system. First, we discuss the convergence of second order perturbation theory and make a comparison to the analytical two particle solution from section 3.1. Second, we present the ground state energy for multiple spin components and the concept of shells is explained. Next, the experiment that we model by Zürn *et al.* [2] is described and the experimentally measured quantity, separation energy, is introduced. Lastly, this chapter compares our numerical result with the experimental data in [2] and we determine the magic numbers.

4.1 Discussion of Numerical Results with Two Spin Components

In an ultracold environment, particles will primarily be in the ground state of the system. If we consider the non-degenerate 1D-QHO, we expect fermions to occupy the lowest energy levels possible from bottom and up in accordance with figure 2.2a. Therefore, it is possible to calculate the ground state energy, with and without a perturbation, as a function of fermion number. The first order energy correction to the ground state $E^{(1)}_{n=0}$ is obtained by computing Case 1 in table 3.1. However, the second order ground state energy correction $E^{(2)}_{n=0}$ from equation (3.17) is more complicated as it is an infinite sum and numerically, this means truncating the sum at some definite cut-off. Though, if there exist a solution which converges, we can extrapolate the results to infinity. We define the cut-off L as the highest 1D-QHO level considered, or highest single-particle excited state taken into account, and compute the overlap integrals in table 3.1. In the extrapolation process, we make the ansatz

$$E^{(2)}_0(L) = a + \frac{b}{L}, \tag{4.1}$$

and fit the parameters a and b to computed data for $L \geq 40$. The result of the extrapolation is shown in figure 4.1a as dashed black lines. We can clearly see how the second order energy correction converges, although more slowly with increasing particle number. The reason for a slower convergence as N increase is because of the additional overlap integrals needed to be computed. By letting the cut-off approach infinity, we extract the energy correction from equation (4.1) as $E^{(2)}_0(L \to \infty)$ and table 4.1 shows the extrapolated second order energy corrections together with the first order energy corrections.

Table 4.1: Results of the first and second order ground state energy corrections with two spin components using perturbation theory.

N	$E^{(1)}_0$	$E^{(2)}_0(L \to \infty)$
2	0.3989	-0.1046
3	0.5984	-0.1097
4	1.0971	-0.1967
5	1.4212	-0.2081
6	2.0009	-0.2857

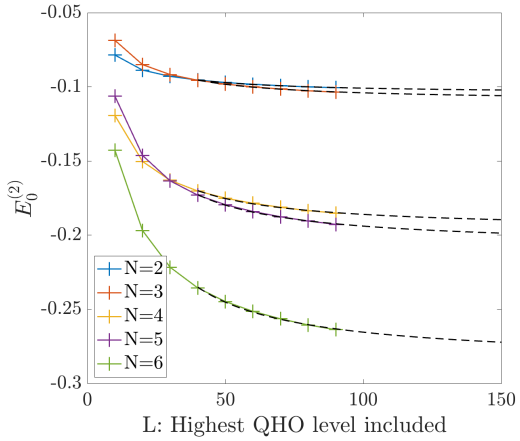

(a) Second order energy correction as a function of the single particle Hilbert space cut-off L.

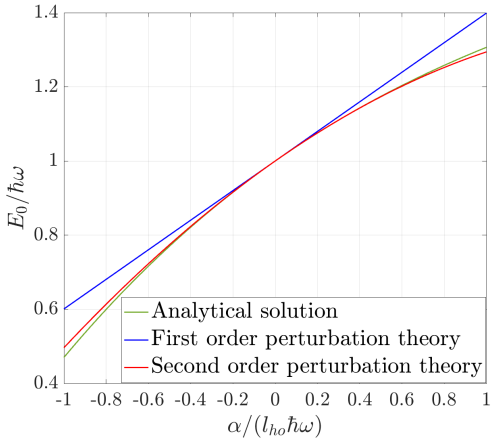

(b) Ground state energy of two particles as a function of the dimensionless interaction strength $\alpha/(l_{ho}\hbar\omega)$.

Figure 4.1: **(a)** contains the calculations of $E_0^{(2)}(L)$ with second order perturbation theory for $N = 2$ to $N = 6$ and power law fits (black dashed lines) according to equation (4.1). We can see an excellent match between our calculations and the fitted power laws. **(b)** is a comparison of our results with perturbation theory to the exact analytical two-particle solution in section 3.1.

Having established the convergence of the second order energy correction, we proceed to compare the results for $N = 2$ in table 4.1 to our two particle analytical solution from section 3.1 in figure 4.1b. We see an excellent agreement for $|\alpha/(l_{ho}\hbar\omega)| < 0.2$ but the solutions deviate as the interaction strength increases. Although, second order perturbation theory agrees very well for interaction strengths up to $|\alpha/(l_{ho}\hbar\omega)| \approx 0.7$. The agreement between perturbation theory and the analytical solution for two particles implies that the numerical results are accurate, and we move on to applying our computed results.

4.2 Ground State Energy and Shells of the 1D-QHO

The ground state energies for two, three and four spin components as a function of particle number are shown in figure 4.2. The non-interacting energy is calculated using equation (2.27) and the energy with interactions is calculated using first order perturbation theory.

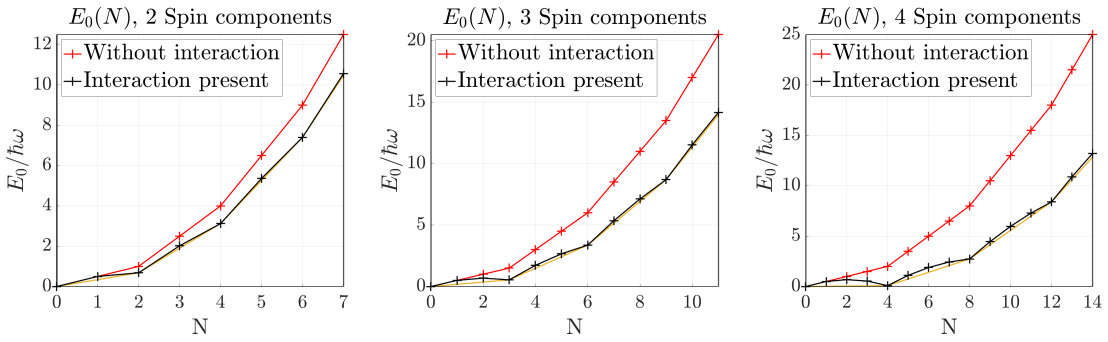

Figure 4.2: The ground state energy with and without interactions as a function of particle number for different numbers of spin components. The dimensionless interaction strength $\alpha/(l_{ho}\hbar\omega)$ is -0.8. We see that the energy is particularly lowered for multiples of the number of spin components when interactions are present. In addition, we note the convexity of the orange lines, i.e. $E_0(N = k\cdot\#\sigma)$ where $k \in \mathbb{N}_0$. The energy is a convex function of particle number without interactions, and convex with multiples of the number of spin components with interactions.

The emergence of shells is already visible without interactions: the slope only changes for multiples of the number of spin components. This shell effect is explained by interpreting a 1D-QHO energy level as a shell, where the increase in energy will be constant while a level is being filled with particles. In order to minimise the ground state energy, particles will occupy the lowest energy levels possible. However, due to Pauli's exclusion principle, a level can only be occupied by particles of different spin components. We therefore observe a constant increase in energy between consecutive multiples of the number of spin components, i.e. shells.

The shell effect is magnified by the interactions and becomes more apparent with more spin components. We also find that energy is no longer a convex function[1] of particle number but instead displays a closed shell effect. This can be observed in figure 4.2 where e.g. $E_0(3) < E_0(2)$ for three spin components and $E_0(4) < E_0(3)$ for four spin components. However, we notice that the orange lines which show $E_0(N = k \cdot \#\sigma)$, with $k \in \mathbb{N}_0$, are still convex functions. This mathematically quantifies the shell effect: the energy of partially filled shells always lie above the orange line, indicating that such configurations of particles are not as strongly bound. That filled shells correspond to a significant decrease in energy, and hence increased stability, can be explained by the interaction energy depending on the overlap between wave functions of different spin. Realising that two fermions of different spin occupying the same 1D-QHO energy state have the same unperturbed spatial wave function, we can expect a significant increase in overlap. The overlap can hence be translated into how much particles interact. With an attractive interaction ($\alpha < 0$), the ground state energy is subsequently decreased. A similar shell effect is observed in nuclear physics where closed shells correspond to particular stable nuclei, i.e. magic numbers [7]. The concept of shells is important when we in the following sections will interpret experimental results.

4.3 Description of the Experiment by Zürn *et al.*

In [2], a few weakly interacting fermions with two spin components (two hyperfine states of ^{6}Li) were prepared in the ground state of a quasi-1D harmonic potential with methods described in section 1.3. The quasi-1D system was created by using a longitudinal frequency $\omega_{||} = 2\pi \cdot 1.488$ kHz and a perpendicular frequency $\omega_\perp/\omega_{||} \approx 10$, making the energy scale $\hbar\omega$ in the longitudinal direction much smaller than in the perpendicular. Thus, a one dimensional treatment of the system is sufficient [15]. To intuitively realise how a quasi-1D system is created, one can consider building the ground state in the experiment described; it is first after 20 atoms (10 atoms of each spin component) that an additional atom could find it energetically favourable to occupy an excited state in the perpendicular direction where the level spacing is $\omega_\perp \approx 10 \cdot \omega_{||}$.

Following the preparation of a fixed number of weakly interacting atoms in the ground state of the trap, a magnetic field gradient was applied, tilting the trapping potential to a well-defined height for a variable time. A tilted trapping potential is illustrated in figure 4.3. By modifying the tilted potential height such that only the most energetic atom could tunnel through the barrier within the experimental timescale, single particle tunnelling rates were measured. The experimentally obtained tunnelling rates were subsequently used to extract a quantity called "separation energy" through an iterative process of matching WKB calculations (a way of approximating solutions to linear differential equations) with experimental data. The separation energy is the energy released as the N^{th} atom tunnels out of the confinement and leaves $N-1$ particles in their ground state. It is defined as

$$E_{\text{sep}}(N) = \left(E_N - E_N^{(0)}\right) - \left(E_{N-1} - E_{N-1}^{(0)}\right), \tag{4.2}$$

where E_N is the ground state energy of an interacting system with N atoms and $E_N^{(0)}$ the non-interacting energy [16]. Separation energy is thus a quantity that gives us information about the interaction strength of the atoms. It can also show increased stability with certain magic numbers of atoms in the trap and pairing effects between atoms.

[1] If a line segment connecting two points on the graph of a function always lies above or on the graph, a function is convex.

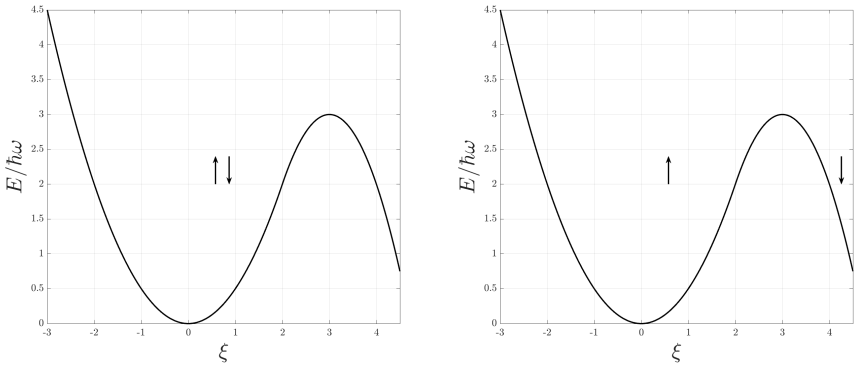

(a) Two atoms of different spin confined.

(b) One atom has tunneled through the barrier.

Figure 4.3: An illustration of the tilted 1D-QHO harmonic potential in the experiment by Zürn *et al.* [2] with two atoms of different spin. In **(a)**, two atoms are confined in the tilted trapping potential whereas in **(b)**, the $\sigma = \downarrow$ atom has tunnelled through the barrier.

4.4 Numerical Results of Calculating the Separation Energy

To reproduce the experimental data in [2], we construct the separation energy as a function of particle number according to equation (4.2) with the results from table 4.1. The interaction strengths α are chosen to minimise χ in equation (4.3), and the result is shown in figure 4.4a.

$$\chi = \sum_{N=2}^{6} \left(E_{\text{sep}}^{\text{calculated}}(N) - E_{\text{sep}}^{\text{experiment}}(N) \right)^2 \tag{4.3}$$

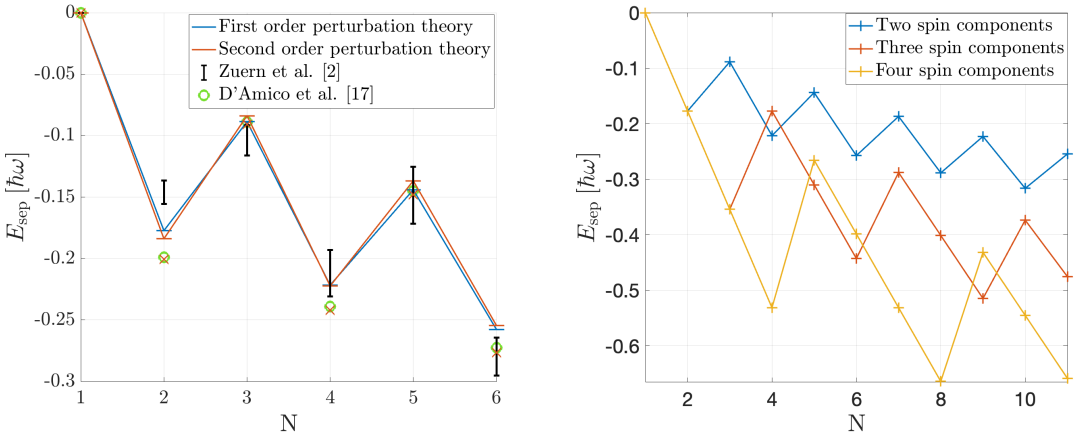

(a) Two spin components

(b) Multiple spin components.

Figure 4.4: Separation energy as a function of particle number. In **(a)** our results with perturbation theory are compared to experimental data by Zürn *et al.* [2], which are shown as black error bars. Bars connected by blue is the first order perturbation theory with the interaction strength $\alpha/(l_{ho}\hbar\omega) = -0.444$ and bars connected by red is the second order perturbation theory with the interaction strength $\alpha/(l_{ho}\hbar\omega) = -0.416$. Furthermore, with $\alpha/(l_{ho}\hbar\omega) = -0.45$, the results from exact diagonalisation in [17] are shown as green circles and our results with second order perturbation theory are shown as red crosses. In **(b)** the first order perturbation theory is used with $\alpha/(l_{ho}\hbar\omega) = -0.444$. We can see spikes in magnitude of the separation energy for multiples of the spin components.

Although the calculated separation energy do not always lie within the experimental uncertainty bars in figure 4.4a, we can see that the qualitative behaviour is successfully reproduced. Furthermore, we find that the first order perturbation theory actually match the experimental data better, but the second order perturbation theory results do not differ by much. This implies that atoms in the experiment are weakly interacting, i.e. the system is only slightly perturbed and perturbation theory is a good approximation. Hence, we expect our model to be a good description of the experiment.

In [17], the Hamiltonian in equation (3.1) was expressed in matrix form and diagonalised. The resulting eigenvalues correspond to the energy of the system, and these are shown as green circles in figure 4.4a. The red crosses that almost perfectly intersect the green circles are our results with second order perturbation when we set the same interaction as was used in [17] i.e. $\alpha/(l_{ho}\hbar\omega) = -0.45$; the first order perturbation hardly changes from what is seen in figure 4.4a. That the second order perturbation theory and exact diagonalisaton are in excellent agreement is also consistent with the comparison between perturbation theory and the analytical two particle solution in figure 4.1b: at $\alpha/(l_{ho}\hbar\omega) = -0.45$ the first order perturbation theory fails to reproduce the analytical solution accurately, whereas the second order perturbation theory succeeds. One reason why our results fail to match experimental data better could be from the anharmonicity of the true level spacing in the confining trap, meaning our harmonic approximation breaks down.

Having established the success of our model, we can now discuss the behaviour observed in figure 4.4a. We can see that for an even number of atoms the magnitude of the separation energy increases, meaning that the system is more stable. This odd-even effect observed is reminiscent of a pairing effect seen in nuclear physics, where an even number of protons or neutrons have larger binding energies, and hence, are more resilient against decay [7]. Despite a nucleus having completely different structures and forces acting between its constituents, compared to the modelled 1D-QHO system, both systems are comprised of fermions which follow Pauli's exclusion principle. Consequently, we see a similar shell effect in both systems. With two spin components, an even number of atoms correspond to filled 1D-QHO shells and as discussed in section 4.2, the ground state energy is significantly lowered for attractive interactions as a consequence. Therefore, a system of an even number of atoms experience an effective higher potential to tunnel through than an odd number of particles. Consequently, a lower tunnelling rate is observed, indicated by figure 4.4a. Another effect seen is a general increase in magnitude of separation energy with the number of atoms. This can be explained by more atoms being able to interact with one another.

In figure 4.4b, the separation energy is calculated using first order perturbation theory, and the result is shown for up to four spin components. The behaviour in figure 4.4b is in accordance with the shell model described in section 4.2. Whenever an atom occupies an energy level (shell) by itself, i.e. $N = k \cdot \#\sigma + 1$, $k \in \mathbb{N}_0$, it interacts less with other atoms and the magnitude of the separation energy is decreased. Another thing worth noting is that the slope is linear within a shell with first order perturbation theory. This can be understood by the pairwise interaction potential: the difference in interaction energy of removing two consecutive particles of different spin is the interaction energy between the first and second particle removed. Detailed calculations for the difference in interaction energy can be found in appendix B (equation (B.3)) and we only state the result here as

$$\Delta E_{\text{sep}}(N) = \frac{\alpha}{l_{ho}} \int \mathrm{d}\xi |\widetilde{\psi}_n(\xi)|^4. \tag{4.4}$$

We find that with first order perturbation theory, the slope within the n^{th} shell is not only linear, but also the same independently of the number of spin components.

Finally, in figure 4.4, we can clearly see spikes in the magnitude of the separation energy when the number of particles equal multiples of the spin components. This strengthens the notion that the shell model used to interpret the experimental results is successful, i.e. a filled shell is more bound. Subsequently, we assign magic numbers to the system of a 1D-QHO with weak attractive interactions as an integer times the number of spin components.

5

Pauli Crystals

Having studied the effect of interactions on the energy of a many-body system, we now initially return to the non-interacting system with one spin component. This chapter introduces the phenomena of Pauli crystals, a natural consequence of the Pauli principle. After a brief introduction to the subject, the chapter will explain the probability density of the many-body wave function and the algorithms used to simulate the Pauli crystals. Then, the crystals will be simulated in both 1D and 2D, successfully verifying very recent experimental results in [3]. Finally, completely new research will be presented that applies perturbation theory to Pauli crystals in 1D.

5.1 Introduction to Pauli Crystals

As mentioned in the background, no two fermions can occupy the same quantum state due to the Pauli principle. One manifestation of the Pauli principle arises when fermions confined to a potential are cooled to a sufficiently low temperature. Due to the principle, the fermions try to maximise the distance between themselves as they are trapped in the bottom of a bowl-shaped potential. This results in the atoms arranging themselves in a sort of crystal pattern known as Pauli crystals. The field is experiencing a recent surge of research, with experimental work done just last year by Holten *et al.* [3] resulting in pictures taken of Pauli crystals, seen in figure 5.6.

Experimentally Pauli crystals can be observed thanks to fluorescent imaging, which revolves around exciting atoms suspended in an optical trap through illumination and collecting the emitted photons when the atoms relax. In [3], this technique was used to take snapshots of the fermions, collapsing the many-body wave function and showing the individual particles. With multiple snapshots, the particles will simply collapse according to their probability density and show no correlation between themselves. It is only following image processing, which is described in detail in [18], [19], that the crystals appear. The aim of this chapter is mainly to recreate the results in [3] by simulating repeated measurements of N particles and then employing the image processing to reveal the particle correlation. To understand the results, we also look at the probability density and most probable positions of the particles. In the end, the simulations should form patterns that reflect the Pauli principle and match the patterns in figure 5.6.

5.2 The Probability Density

For one particle the probability density is simply $\left|\psi(x)\right|^2$. However, for many particles there are multiple probability densities depending on whether or not it is taken into consideration how the particles are correlated, i.e. how they are placed in relation to each other [20]. The highest order correlation gives the probability of finding N particles at given positions. However, for visualisation it is sufficient to use the first order correlation, i.e. the probability density, which display the probability of finding a particle at a given position r.
We introduce the density operator

$$\hat{n}_\sigma(r) = \sum_{i=1}^{N_\sigma} \delta(r - \hat{x}_{\sigma i}) \tag{5.1}$$

and insert it into $\langle\Psi|\,\hat{n}_\uparrow(r)\,|\Psi\rangle$ to obtain the probability density. Details concerning the derivation of this expression is given in appendix B.3 and given here is only give the final result

$$\langle\Psi|\,\hat{n}_\sigma(r)\,|\Psi\rangle = \sum_{i=1}^{N_\sigma} |\psi_{n_{\sigma i}}(r)|^2. \tag{5.2}$$

As can be seen, the probability density at position r is simply the sum of one-particle wave functions for one spin species, meaning that it has lost the information regarding how the particles are correlated.

5.3 Algorithms

The Pauli crystals were simulated using two algorithms: The Monte Carlo Algorithm and the Metropolis algorithm [21], where the former can be considered a special case of the latter. The Monte Carlo algorithm is a Markov chain that aims to find the most probable particle positions. In contrast, the Metropolis algorithm instead samples the the wave function, offering particle positions with different probabilities and simulating experimental measurements.

5.3.1 Monte Carlo Algorithm

The Monte Carlo algorithm works by using the highest order correlation of probability density $\left|\Psi(\vec{r}_1, ..., \vec{r}_N)\right|^2$ for N particles in order to keep the information about the particles relation to each other and maximising it. This gives the most probable positions for the particles. The most probable outcome is important since it firstly gives an indication of where the Pauli crystals will form and and how they will arrange themselves, and secondly, is required for making the angular corrections needed in 2D, discussed more in section 5.5. At the start of each measurement of N particles, the algorithm assigns all particles random positions $\vec{r}_{start}$ within the interval $\xi \in [-10, 10]$ in 1D, or in a circle square with the radius five in 2D. Then, a new set of positions are randomised for all particles $\vec{r}_{new}$ within an interval 2λ in 1D, or a square of side length 2λ in 2D, where lambda is a parameter chosen so that the particles converge to their most probable positions. The probabilities $|\Psi|^2$ of the those two positions are calculated, and a comparison is made to check whether the new probability is higher. If it is, the new configuration $\vec{r}_{new}$ is set as the starting point for the next iteration. Otherwise the next iteration is repeated with the same starting positions as before, $\vec{r}_{start}$. With a sufficient number of iterations i and a well chosen λ, the probability converges to the most probable positions, in our case with $\lambda = 10^{-2}$ and i=10^4.

5.3.2 The Metropolis algorithm

The Metropolis algorithm works very similarly to the Monte Carlo algorithm, but adds one extra if-statement if the probability is lower after moving the particles within the interval 2λ. We call the quotient between the new probability and the old probability after a move p. If the new probability is lower than the old and $p < 1$, there is still a chance p that the particles move to the new position. Furthermore, there is a probability $(1 - p)$ that the particles stay in their old positions for the next iteration, similarly to how the Monte Carlo algorithm works. This results in more spread out measurements where the particles are unlikely to end up in either the most probable positions or really improbable positions, mimicking real life measurements. [18], [21]

5.4 Simulating Pauli crystals in 1D

The probability density and introduced algorithms will now be employed to simulate Pauli crystals and explain theoretically why they appear. The process will first be done in 1D and then repeated in 2D. Using equation (5.2) we plot the probability density in blue for one spin species in figure 5.1 for three and six particles. In the same figure, we also plot the most probable positions in red for three and six particles using the Monte Carlo algorithm. It is noteworthy how the number of peaks in the figures corresponds to the number of particles, and the fact that the particles in their most

probable outcome closely align with those peaks. The number of peaks in the probability density give an indication that the particles might not occupy the same position in 1D space, despite the probability density containing no information on particle correlation. The most probable outcome then confirms it by placing the particles evenly, as to maximise the distance between them in the potential, clearly obeying the Pauli principle.

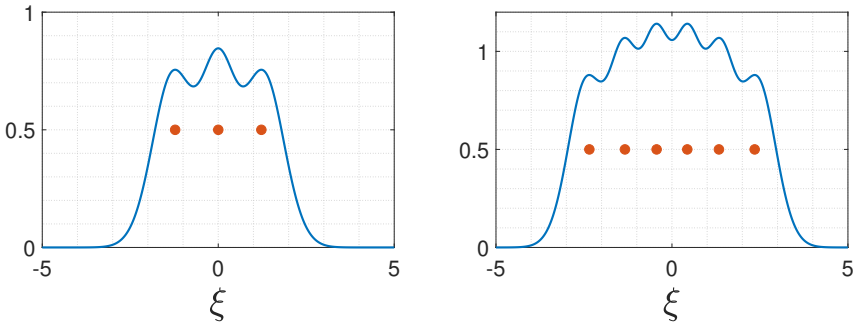

(a) Three particles. **(b)** Six particles.

Figure 5.1: Plots of the most probable configurations for three and six particles in 1D. The blue lines are the probability densities and the red dots are the particles in their most probable configuration.

In order to simulate real measurements, we employ the Metropolis algorithm. Due to the Law of large numbers [22, p. 177-178], which dictates that a large number of measurements are required to achieve convergence, 10^5 measurements are used. These form the histogram in 5.2a for three particles with no clear pattern. This is because of quantum fluctuations in position and to reveal the correlation between particles, the centre of mass for each measurement is calculated as $\xi_{CoM} = 1/N \sum_i \xi_i$ and then aligned with $\xi = 0$. The results can be seen in figure 5.2b. The three peaks verify that the wave functions collapses in accordance with its probability density, figure 5.1a, and that the Metropolis algorithm is capable of simulating it. A parallel can be drawn between these simulations and the double-slit experiment, where the purpose is to demonstrate the wavelike properties of particles through interference and observe a distribution which is only made visible after many measurements.

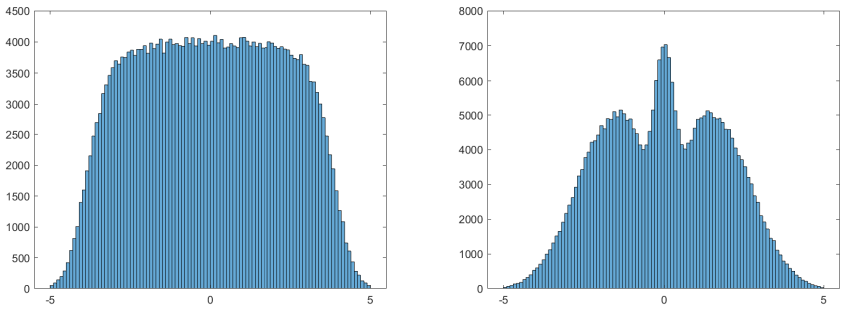

(a) Histogram of measurements for three particles. **(b)** Centre of mass corrections.

Figure 5.2: Histogram of the measured positions for three particles for 10^5 measurements.

5.5 Pauli Crystals in 2D

Having simulated the Pauli crystals in 1D, we move onto the 2D case where we will verify the experimental results in figure 5.6 theoretically. First, we need to define some basic characteristics

of the dimensionless harmonic oscillator in two dimensions. The coordinates in two dimensions are x and y and their dimensionless equivalents are $\xi = x/l_{ho}$ and $\eta = y/l_{lo}$, respectively. The single-particle wave function for the harmonic oscillator in two dimensions becomes a product of two 1D wave functions with an adjusted normalisation constant:

$$\tilde{\psi}_{n_\xi n_\eta}(\xi, \eta) = \frac{1}{\sqrt{2^{n_\xi + n_\eta} n_\xi! n_\eta! \sqrt{\pi}}} \mathrm{e}^{-(\xi^2+\eta^2)/2} H_{n_\xi}(\xi) H_{n_\eta}(\eta). \tag{5.3}$$

An additional challenge in 2D is the degeneracy briefly mentioned in section 2.2. It means that only filled shells with 1, 3, 6, 10, 15,... particles are non-degenerate and can be simulated. In addition, the wave function exhibits a rotation symmetry in the ground state. Hence, angular corrections are necessary to view the Pauli crystals.

5.5.1 Simulating Pauli Crystals in 2D

The 2D probability density for one, three and six particles can be viewed in figure 5.3, where we can see circles forming where it is more likely to find a particle. However, very little can be said about the correlation of the particles. The relationship between the particles only becomes clear after inspecting the most probable positions for one, three and six particles in figure 5.4, plotted by using the Monte Carlo algorithm. There we see that the particles form circular shells to try to maximise the distance between themselves. It is tempting to draw parallels between this and the shells formed by magic numbers. Although, as was pointed out in [20], the number of shells in Pauli crystals do not correspond to the number of degenerate energy levels in the system, nor do the shells in the Pauli crystals have the same number of particles in each shell as would be expected for the magic numbers.

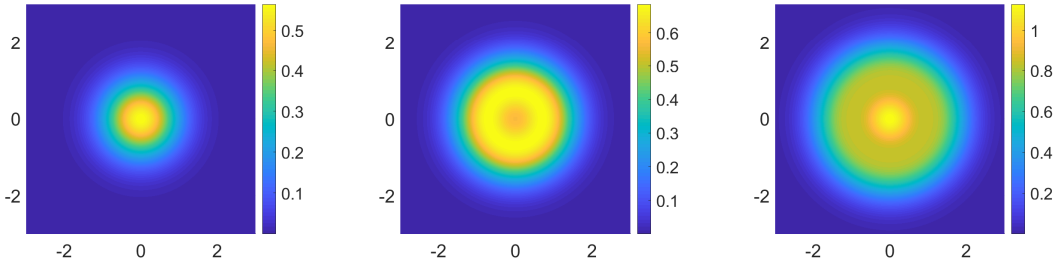

(a) One particle. **(b)** Three particles. **(c)** Six particles

Figure 5.3: The probability densities in 2D for one, three and six particles.

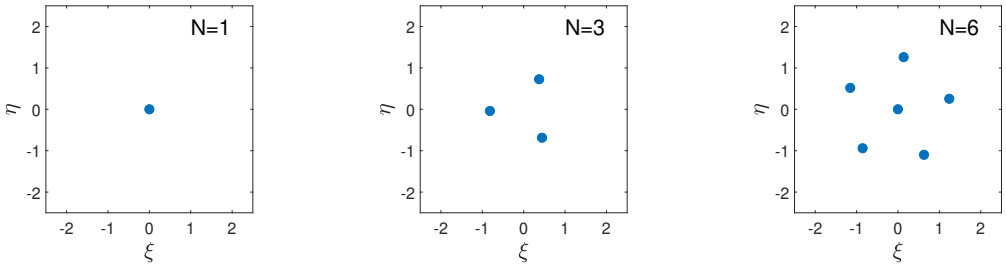

(a) One particle. **(b)** Three particles. **(c)** Six particles.

Figure 5.4: The blue dots represent the most probable configuration for one, three and six particles in 2D. The particles clearly obey the Pauli exclusion principle, trying to maximise their distance and forming circular shells.

Keeping the probability density and the most probable outcome in mind, we simulate experimental measurements by using the Metropolis algorithm in 2D. Without any image processing, quantum

fluctuations in the particles positions once again lead to histograms without any clear patterns. However, by using the same centre of mass correction as in the 1D-case, we obtain the plots 5.5a and 5.5c for three and six particles, respectively. As can be seen, the Metropolis algorithm clearly samples the wave function in accordance with its probability density in figure 5.3 and verifies the experimental measurement in figure 5.6a for three particles.

To see the actual Pauli crystals in 2D, we also need to perform angular corrections for each measurements. Firstly, each measurement $\vec{r}$ is transformed into polar coordinates and the particles in a measurement, with coordinates $\vec{r_i} = (r_i, \phi_i)$, are sorted by decreasing angle ϕ_i. Secondly, each particle in a measurement is assigned to a particle from the most probable outcome in figure 5.4, with the coordinates $\vec{r}_{prob,i} = (r_{prob,i}, \phi_{prob,i})$. Finally, each measurement is rotated as to best align with the most probable outcome. This is done by finding the angle θ that minimises

$$d = \sum_{i=1}^{N} \left(\phi_i - \phi_{prob,i}\right)^2. \tag{5.4}$$

The results can be viewed in figures 5.5b and 5.5d. As can clearly be seen, the crystals form around the most probable positions, as showcased in the figures of 5.4. Furthermore, when comparing this to the experimental results in 5.6 we can safely say that our models and algorithms have successfully simulated the experimental results.

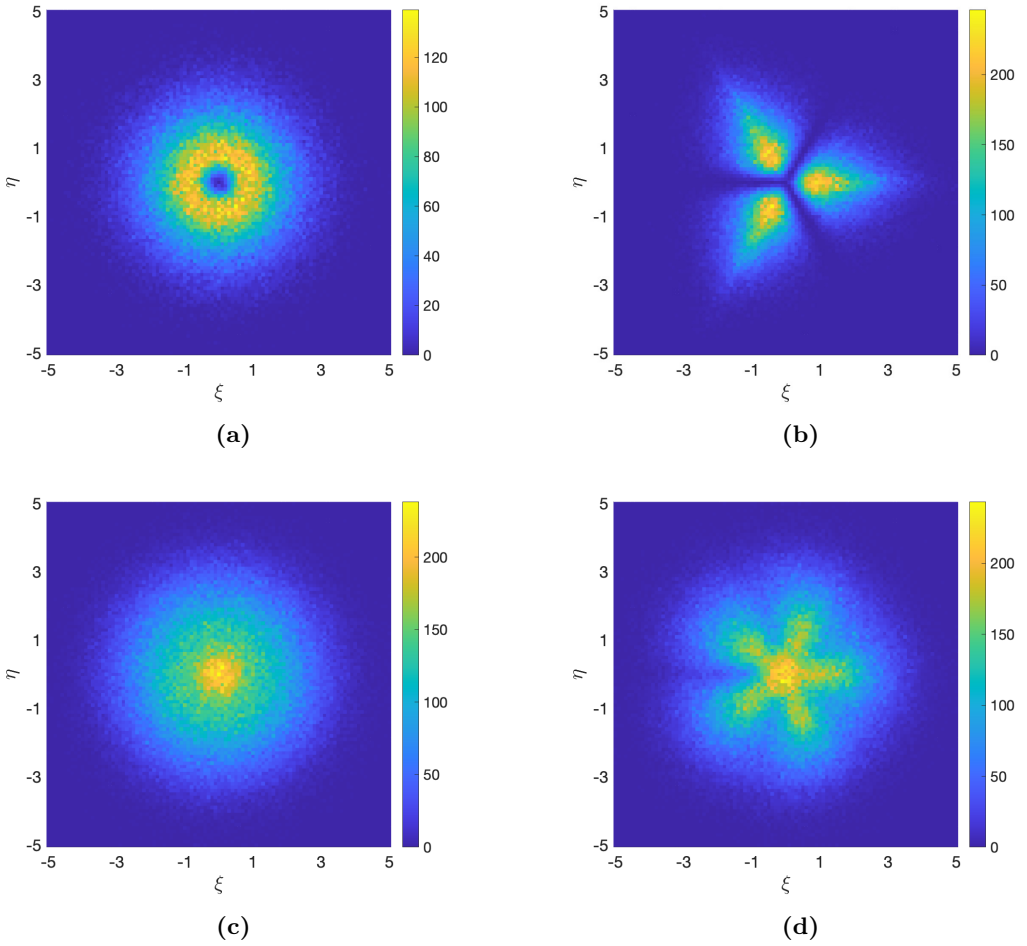

Figure 5.5: The left side shows histograms of $5 \cdot 10^4$ measurements for three and six particles gained from the Metropolis algorithm with centre of mass corrections. The right side shows the same measurements after angular corrections were made.

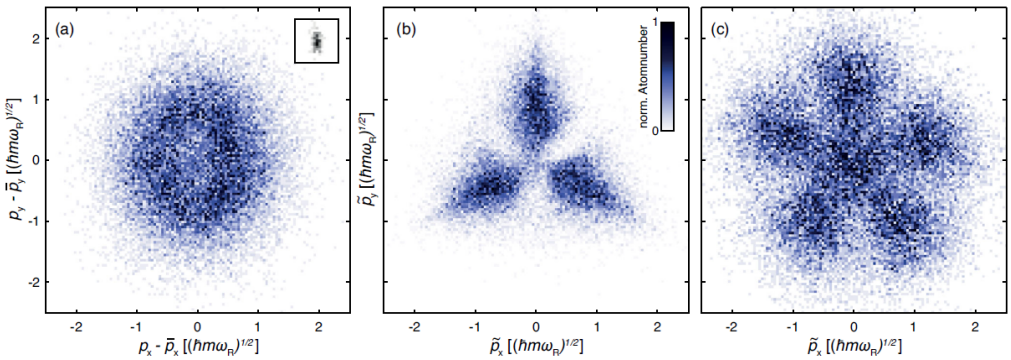

Figure 5.6: Experimental measurements showing Pauli crystals in [3]. Figure (a) shows the single-particle density in a 2D histogram without implementation of angular corrections. Figures (b) and (c) are the histograms with angular corrections for three and six particles.

5.6 Perturbing the Crystals in 1D

The previous sections studied Pauli crystals as they naturally arise without interactions and explained experimental results. In this section we will cover new theoretical ground by studying how the Pauli crystals in one dimension are affected when interactions are added between two spin components. This is done by combining the results from section 3.3 with the Monte Carlo algorithm and adding the first order correction of the wave function to the unperturbed wave function in 1D as $\Psi = \Psi^{(0)} + \alpha\Psi^{(1)}$. α is the interaction strength and $\Psi^{(1)}$ is given by equation (3.16) with the sum truncated at 20 excited states. This is done to reduce computing time and is deemed viable as the goal is to study the general effect of interactions, rather than simulate exact expected results.

The Monte Carlo algorithm is again used in order to maximise the probability $|\Psi|^2$. However, there is an issue with the results not always converging towards a single, most probable position. The issue is reduced with larger $\lambda \approx 1$, though not completely alleviated. The most likely explanation for the less likely outcomes is that the algorithm gets stuck in local maximums of the wave function, arising because of the excited states added from first order correction. The issue might possibly be removed completely with an adaptable λ, although we leave this to future studies due to time constraints. The most probable positions are shown in figure 5.7 for two, three four and five particles. Spin up and down particles and their unperturbed probability densities are marked with blue and red, respectively. Furthermore, the spin down particles have been made slightly bigger than the spin up particles to visualise potential overlap. Note that a negative α means attraction and a positive repulsion between particles of different spin. Particles of the same spin do not interact by the delta potential, as shown in appendix A.

Let us first study the case with two and four particles in figure 5.7a and 5.7c, with the same number of particles in the spin up and spin down state. For $\alpha = 0$ and $\alpha < 0$ the results are the same, since the spin up and spin down particles have the same shaped probability density, and the attractive interaction cannot bring the particles any closer than they already are in the unperturbed case. However, for $\alpha > 0$, the particles repel each other, occupying equidistant positions from the peaks in the probability density. This was expected, as the particles are confined by the symmetric potential while being repelled by each other. For three and five particles in figure 5.7b and 5.7d, the particles align with the peaks of their probability densities in the unperturbed case as expected. Repulsive interactions simply increases the distance between the particles. However, attractive interactions are particularly interesting as the spin up and spin down particles seem to form the beginning of pairs, with one particle being left out for odd N.

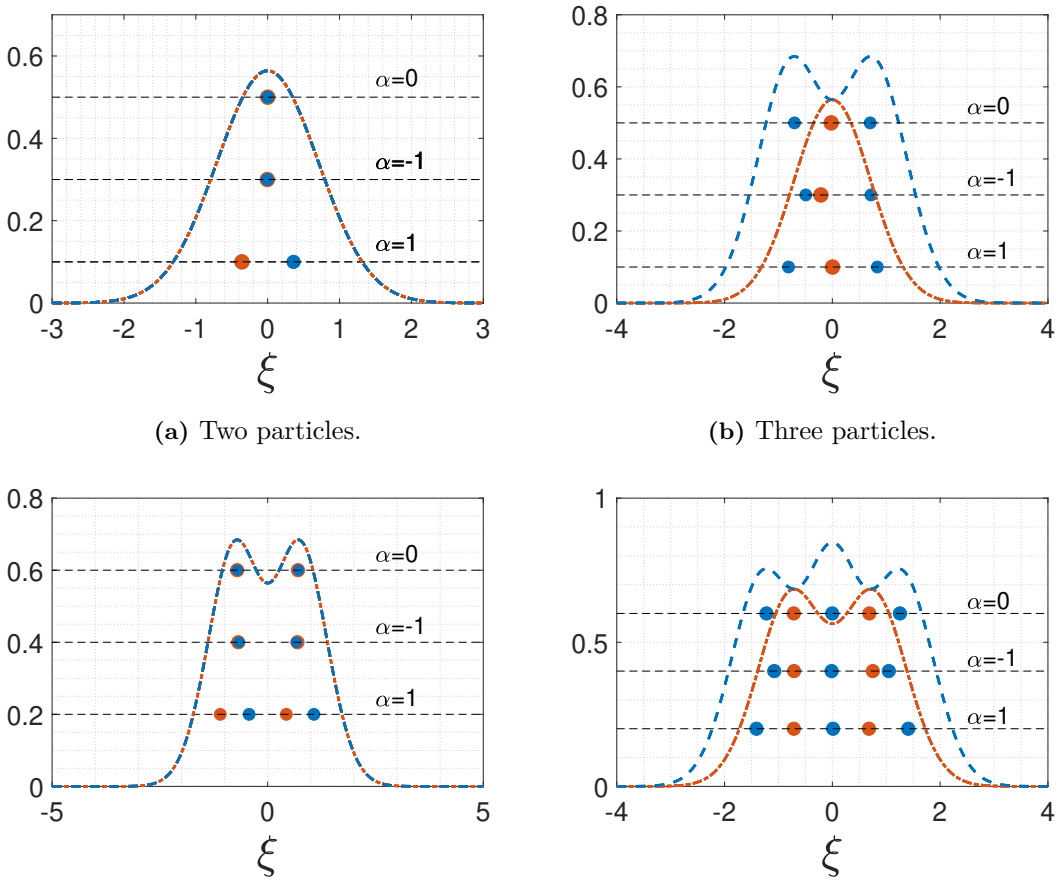

(a) Two particles.

(b) Three particles.

(c) Four particles.

(d) Five particles.

Figure 5.7: Most probable configuration for two, three, four and five particles in the ground state with different values of α. Spin up and down particles and their unperturbed probability densities are marked with blue and red, respectively. $\alpha = 0$, means no interactions between particles. $\alpha < 0$ and $\alpha > 0$ means attractive and repulsive interactions, respectively, between particles of different spin.

6
Conclusions

This chapter summarises what has been achieved in the thesis and presents possible future applications and new fields of study. The goal of the thesis was to recreate the experimental results in Zürn *et al.* [2] and Holten *et al.* [3] and hence, simulate patterns in an interacting quantum gases, specifically pairing, magic numbers, and Pauli crystals.

6.1 Interactions in a 1D Few-Fermion Gas

We introduced our model of a few fermions in a harmonic potential in one dimension, where particles of different spin interact with a zero-point potential. The energy of such a system was calculated analytically for two particles and two spins, and numerically with perturbation theory for multiple particles and multiple spins. From these calculations we can draw a number of conclusions. Firstly, the analytical and numeric results are in agreement, supporting that the calculations with perturbation theory are correct. Secondly, a visible shell effect emerged for the non-interacting system, which was made even more visible by adding interactions. From this, we could see the magic numbers, which corresponded to multiples of the number of spin components in the system. Finally and most importantly, the energies calculated with perturbation theory matched the experimental results in [2], confirming the validity of our model and showing a clear pairing effect between the fermions. In addition, our results for the second order perturbation theory almost perfectly matched the theoretical work done in [17].

Having established the success of our model, a generalisation to higher dimensions is appealing to future research. The recent experimental advancements make an ideal playground for testing theoretical models; just last year, Bayha *et al.* [9] prepared a two dimensional system of interacting ultracold fermions. Thus, exploring interactions in two dimensions is a promising area for future research. Furthermore, it would be interesting to study the correlation between a more pronounced shell effect in 2D and interactions.

6.2 Pauli Crystals

In the section on Pauli crystals, we gained an understanding of how Pauli crystals are formed by studying the probability density and simulating the crystals in 1D. Furthermore, we successfully simulated the experimental measurements in [3] by using the Monte Carlo and Metropolis algorithms, verifying our model. Finally, we conducted original research, showing how interactions between two spin states likely affect Pauli crystals in one dimension. In conclusion, we have shown that simulating Pauli crystals is not only possible, but gives accurate recreations of experimental data. This provides a foundation for further research to expand upon, such as incorporating higher dimensions [23], simulating a greater number of particles, new interaction models, introduce heavier atoms or even simulate fermionic molecules [24].

Bibliography

[1] J. E. Thomas and M. E. Gehm, "Optically Trapped Fermi Gases", *American Scientist*, vol. 92, no. 3, May/June 2004.

[2] G. Zürn et al., "Pairing in few-fermion systems with attractive interactions", *Phys. Rev. Lett.*, vol. 111, no. 17, Oct. 2013, doi: 10.1103/PhysRevLett.111.175302.

[3] M. Holten et al., "Observation of Pauli Crystals", *Phys. Rev. Lett.*, vol. 126, no. 2, Jan. 2021, doi: 10.1103/PhysRevLett.126.020401.

[4] D. J. Griffiths and D. F. Schroeter, *Introduction to Quantum Mechanics*. 3rd ed., Cambridge, UK: Cambridge University Press, 2018.

[5] L. Pitaevskii and S. Stringari, *Bose-Einstein Condensation and Superfluidity*. Oxford, UK: Oxford University Press, 2016.

[6] L. S. Sparke and J. S. Gallagher III, *Galaxies in the Universe: An Introduction*. 2nd ed., Cambridge, UK: Cambridge University Press, 2007.

[7] B. R. Martin and G. Shaw, *Nuclear and Particle Physics An Introduction*, 3rd edi., Hoboken, New Jersey, USA: Wiley-Blackwell, Apr. 2019.

[8] V. Bekassy and C. Lundqvist, *Magic_Numbers*. Available: `https://github.com/CarinLundqvist/Magic_Numbers`.

[9] L. Bayha et al., "Observing the emergence of a quantum phase transition – shell by shell", *Nature*, vol. 587, pp. 583–587, Nov. 2020, doi: 10.1038/s41586-020-2936-y.

[10] D. V. Schroeder, *An Introduction to Thermal Physics*. Boston, USA: Addison Wesley Longman, 2000.

[11] W. Busch, B. G. Englert, K. Rzążewski and M. Wilkens, "Two Cold Atoms in a Harmonic Trap", *Foundations of Physics*, vol. 28, pp. 549–559, April 1998, doi: 10.1023/A:1018705520999.

[12] G. Zürn, "Few-fermion systems in one dimension", Ph.D. Thesis, Physikalisches Institut, Ruprecht-Karls-Universit at Heidelberg, Heidelberg, Germany, Dec. 2012. [Online]. Available: https://www.researchgate.net/publication/280663724

[13] A. Erdélyi, W. Magnus, F. Oberhettinger and F. G. Tricomi, "Generating Functions" in *Higher Transcendental Functions: Volume 3*, A. Erdélyi, Ed. New York, USA: McGraw-Hill Book Company, Inc., 1955, ch. 19, pp. 250.

[14] M. Abramowitz and I. A. Stegun, *Handbook of Mathematical Functions With Formulas, Graphs, and Mathematical Tables*, 10th ed., Washington DC, USA: National Bureau of Standards Applied Mathematics Series 55, 377-378, Dec. 1972.

[15] Z. Idziaszek and T. Calarco, "Two atoms in an anisotropic harmonic trap", *Phys. Rev. A*, vol. 71 , no. 5, May. 2005, doi: 10.1103/PhysRevA.71.050701.

[16] J. Hofmann, A. M. Lobos and V. Galitski, "Parity effect in a mesoscopic Fermi gas", *Phys. Rev. A*, vol. 93, no. 6, Jun. 2016, doi: 10.1103/PhysRevA.93.061602.

[17] P. D'Amico and M. Rontani, "Pairing of few Fermi atoms in one dimension", *Phys. Rev. A.*, vol. 91, no. 4, Mar. 2015, doi: 10.1103/PhysRevA.91.043610.

[18] M. Gajda, J. Mostowski, T. Sowiński and M. Załuska-Kotur, "Single-shot imaging of trapped Fermi gas", *EPL*, vol. 115, no. 2, Aug. 2016, doi: 10.1209/0295-5075/115/20012.

[19] D. Rakshit, J. Mostowski, T. Sowiński, M. Załuska-Kotur and M. Gajda, "On the observability of Pauli crystals in experiments with ultracold trapped Fermi gases", *Scientific Reports*, vol. 7, no. 15004, Nov. 2017, doi: 10.1038/s41598-017-14952-2.

[20] M. Gajda, J. Mostowski, M. Pylak, T. Sowiński and M. Załuska-Kotur, "Pauli Crystals–Interplay of Symmetries", *Symmetry*, vol. 12, no. 11, p. 1886 , Aug. 2016, doi: 10.3390/sym12111886.

[21] N. Metropolis, A. W. Rosenbluth, M. N. Rosenbluth, A. H. Teller and E. Teller, "Equation of State Calculations by Fast Computing Machines", *J. Chem. Phys.*, vol. 21, no. 6, 1953, doi: 10.1063/1.1699114.

[22] J. A. Rice, *Mathematical Statistics and Data Analysis*, 3rd ed., Pacific Grove, California, USA: Brooks/Cole, 2006.

[23] O. Ciftja and J. Batle, "Statistical interaction description of Pauli crystals in two-dimensional systems of harmonically confined fermions", *Annalen der Physik*, vol. 532, no. 10, Oct. 2019, doi: 10.1002/andp.201900075.

[24] T. Zelevinsky, "Ultracold and unreactive fermionic molecules", *Science*, vol. 363, no. 6429, Feb. 2019, doi: 10.1002/andp.201900075.

A

Showing that Particles with Same Spin do Not Interact

In order to prove that particles of the same spin do not interact in our model, we will calculate the perturbed energy in a system with one spin component and N particles. The interaction that will be treated as the perturbation is

$$\alpha\hat{H}' = \frac{1}{2}\sum_{i=1}^{N}\sum_{j=1}^{N}\alpha\delta(x_i - x_j). \tag{A.1}$$

Since the particles are indistinguishable, we divide the Hamiltonian by two because every particle is counted twice. We will calculate the first order perturbation energy $E^{(1)}$ and by inserting the compact Slater determinant (2.15) into the expression for the perturbed energy and simplifying we get

$$\begin{aligned}\alpha E^{(1)} =& \langle\Psi|\,\alpha\hat{H}'\,|\Psi\rangle \\ =& A\sum_{i,j=1}^{N}\int \mathrm{d}x_i\,\mathrm{d}x_j\,\psi^*_{n_{p(i)}}(x_i)\psi^*_{n_{p(j)}}(x_j)\delta(x_i - x_j)\psi_{n_{\tilde{p}(i)}}(x_i)\psi_{n_{\tilde{p}(j)}}(x_j) \\ &\times\prod_{l\neq i,j}\int \mathrm{d}x_l\,\psi^*_{n_{p(l)}}(x_l)\psi_{n_{\tilde{p}(l)}}(x_l)\end{aligned} \tag{A.2}$$

A is the factor $\alpha/2N!\sum_{p,\tilde{p}\in S_N}\mathrm{sign}(p)\,\mathrm{sign}(\tilde{p})$. The delta function operates on the second line in (A.2), while the orthonormality of the wave function turns the scalar product on the final line in into $\delta_{p(l)\tilde{p}(l)}$. For the product of Kronecker deltas to be non-zero the condition is that $p(l) = \tilde{p}(l)$ for $l \neq i, j$, resulting in either

$$\begin{cases} p(i) = \tilde{p}(i) \\ p(j) = \tilde{p}(j) \end{cases} \quad \text{or} \quad \begin{cases} p(i) = \tilde{p}(j) \\ p(j) = \tilde{p}(i) \end{cases} \tag{A.3}$$

However, due to the anti-symmetry of the Slater determinant, interchanging two elements in a permutation leads to a sign change. Hence, the final result including $N!\cdot 2$ terms is

$$\alpha E^{(1)} = \frac{\alpha}{2N!}\sum_{\tilde{p}\in S_N}(\pm 1\mp 1)\,\mathrm{sign}(\tilde{p})\sum_{i,j=1}^{N}\int \mathrm{d}x_j\,|\psi_{n_{\tilde{p}(i)}}(x_j)|^2|\psi_{n_{\tilde{p}(j)}}(x_j)|^2 \equiv 0. \tag{A.4}$$

The result shows the Pauli exclusion principle manifesting itself; two identical fermions cannot occupy the same spatial position, making the perturbed energy zero. Thus, the energy for a single-component system is the same as for a non-interacting two-component system: the sum of single particle energies $E = \sum_{i=1}^{N}\varepsilon_i$. This has shown that particles of the same spin do not interact via delta function interactions.

B

Complete Relevant Calculations

This appendix includes calculations that are deemed not necessary to understand the thesis, but which we have derived ourselves in order to obtain results. It can be of a pedagogical value for the interested reader. The sections are unrelated to each other.

B.1 Overlap Calculation

This sections shows some steps in the derivation of the overlap integrals from section 3.3 that are excluded from the chapter. Firstly, a step in the derivation for the overlap integral in case two (equation (3.21)):

$$\begin{aligned}\langle\Psi|\,\hat{H}'|\Psi'\rangle =&\frac{1}{N_\uparrow!N_\downarrow!}\sum_{p\in S_{N_\uparrow-1}}\text{sign}^2(p)\sum_{\tilde{p}\in S_{N_\downarrow}}\text{sign}^2(\tilde{p})\\ &\times\sum_{i=1}^{N_\uparrow}\sum_{j=1}^{N_\downarrow}\int \mathrm{d}x_{\downarrow j}\,\psi^*_{n_\gamma}(x_{\downarrow j})\psi_{n_\beta}(x_{\downarrow j})|\psi_{n_{\tilde{p}(j)}}(x_{\downarrow j})|^2\\ =&\frac{(N_\uparrow-1)!N_\downarrow!N_\uparrow}{N_\uparrow!N_\downarrow!}\sum_{j=1}^{N_\downarrow}\int \mathrm{d}x_{\downarrow j}\,\psi^*_{n_\gamma}(x_{\downarrow j})\psi_{n_\beta}(x_{\downarrow j})|\psi_{n_{\tilde{p}(j)}}(x_{\downarrow j})|^2\\ =&\frac{1}{l_{ho}}\sum_{j=1}^{N_\downarrow}\int \mathrm{d}\xi\,\widetilde{\psi}^*_{n_\gamma}(\xi)\widetilde{\psi}_{n_\beta}(\xi)|\widetilde{\psi}_{n_j}(\xi)|^2.\end{aligned}\tag{B.1}$$

Case three in equation (3.21) follow in the exact same manner as above. Secondly, steps in the derivation for the overlap integral in case four:

$$\begin{aligned}\langle\Psi|\,\hat{H}'|\Psi'\rangle =&\frac{1}{N_\uparrow!N_\downarrow!}\sum_{p\in S_{N_\uparrow-1}}\text{sign}^2(p)\sum_{\tilde{p}\in S_{N_\downarrow-1}}\text{sign}^2(\tilde{p})\sum_{i=1}^{N_\uparrow}\sum_{j=1}^{N_\downarrow}\\ &\times\int \mathrm{d}x_{\downarrow j}\,\psi^*_{n_\gamma}(x_{\downarrow j})\psi^*_{n_\zeta}(x_{\downarrow j})\psi_{n_\beta}(x_{\downarrow j})\psi_{n_\eta}(x_{\downarrow j})\\ =&\frac{(N_\uparrow-1)!(N_\downarrow-1)!N_\uparrow N_\downarrow}{N_\uparrow!N_\downarrow!}\int \mathrm{d}x\,\psi^*_{n_\gamma}(x)\psi^*_{n_\zeta}(x)\psi_{n_\beta}(x)\psi_{n_\eta}(x)\\ =&\frac{1}{l_{ho}}\int \mathrm{d}\xi\,\widetilde{\psi}^*_{n_\gamma}(\xi)\widetilde{\psi}^*_{n_\beta}(\xi)\widetilde{\psi}_{n_\zeta}(\xi)\widetilde{\psi}_{n_\eta}(\xi).\end{aligned}\tag{B.2}$$

B.2 Separation Energy

The calculation of the slope in separation energy within a shell. If we assume the $N_{\sigma'}$th particle of spin σ' is removed, followed by the $N_{\sigma''}$th particle of spin σ'', equation (4.2) can together with

equation (3.27) be written as

$$\begin{aligned}\Delta E_{\text{sep}}(N) &= E_{\text{sep}}(N) - E_{\text{sep}}(N-1) \\ &= \sum_{\sigma\neq\sigma',\sigma''}\sum_{i=1}^{N_\sigma}\frac{\alpha}{l_{ho}}\int \mathrm{d}\xi|\widetilde{\psi}_{n_{\sigma i}}(\xi)|^2\left(|\widetilde{\psi}_{n_{\sigma' N_{\sigma'}}}(\xi)|^2 - |\widetilde{\psi}_{n_{\sigma'' N_{\sigma''}}}(\xi)|^2\right) \\ &+ \sum_{i=1}^{N_{\sigma''}}\frac{\alpha}{l_{ho}}\int \mathrm{d}\xi|\widetilde{\psi}_{n_{\sigma'' i}}(\xi)|^2|\widetilde{\psi}_{n_{\sigma' N_{\sigma'}}}(\xi)|^2 \\ &- \sum_{i=1}^{N_{\sigma'}-1}\frac{\alpha}{l_{ho}}\int \mathrm{d}\xi|\widetilde{\psi}_{n_{\sigma' i}}(\xi)|^2|\widetilde{\psi}_{n_{\sigma' N_{\sigma''}}}(\xi)|^2\end{aligned} \tag{B.3}$$

where the constraint is $\sum_\sigma \sum_{i=1}^{N_\sigma} = N$. Hence, if particles within a shell is removed, the wave functions $\psi_{n_{\sigma'' i}}(\xi) = \psi_{n_{\sigma' i}}(\xi)$, especially $n_{\sigma' N_{\sigma'}} = n_{\sigma'' N_{\sigma''}} = n$, the single particle wave function of the n th shell. Equation (B.3) thus becomes

$$\Delta E_{\text{sep}}(N) = \frac{\alpha}{l_{ho}}\int \mathrm{d}\xi|\widetilde{\psi}_n(\xi)|^4, \tag{B.4}$$

B.3 Density Operator

Here, we do a derivation leading up to equation (5.2) in section 5.2. Using the density operator defined in that section, the probability density is calculated as

$$\begin{aligned}\langle\Psi|\,\hat{n}_\uparrow(r)\,|\Psi\rangle &= \prod_{k=1}^{N_\downarrow}\prod_{l=1}^{N_\uparrow}\int \mathrm{d}x_{\downarrow k}\,\mathrm{d}x_l\,{}^{\downarrow}\Psi^*(x_{\downarrow k})^{\uparrow}\Psi^*(x_{\uparrow l})\hat{n}_\uparrow(r)^{\downarrow}\Psi(x_{\downarrow k})^{\uparrow}\Psi(x_{\uparrow l}) \\ &= \prod_{k=1}^{N_\downarrow}\int \mathrm{d}x_{\downarrow k}\,{}^{\downarrow}\Psi^*(x_{\downarrow k})^{\downarrow}\Psi(x_{\downarrow k})\prod_{l=1}^{N_\uparrow}\int \mathrm{d}x_l\,{}^{\uparrow}\Psi^*(x_{\uparrow l})\hat{n}_\uparrow(r)^{\uparrow}\Psi(x_{\uparrow l}).\end{aligned} \tag{B.5}$$

The inner product of the spin down states becomes **1** due to orthonormality. The expression for the density operator is is inserted and the spin up states are expressed as compact Slater determinants given in equation (2.20):

$$\begin{aligned}\langle\Psi|\,\hat{n}_\uparrow(r)\,|\Psi\rangle &= \mathbf{1}\cdot\frac{1}{N_\uparrow!}\sum_{p,\tilde{p}\in S_{N_\uparrow}}\mathrm{sign}(p)\,\mathrm{sign}(\tilde{p})\sum_{i=1}^{N_\uparrow} \\ &\times\int \mathrm{d}x_{\uparrow i}\,\psi^*_{n_{\uparrow p(i)}}(x_{\uparrow i})\delta(r-x_{\uparrow i})\psi_{n_{\uparrow\tilde{p}(i)}}(x_{\uparrow i})\prod_{l\neq i}\int \mathrm{d}x_{\uparrow l}\,\psi^*_{n_{\uparrow p(l)}}(x_{\uparrow l})\psi_{n_{\uparrow\tilde{p}(l)}}(x_{\uparrow l}).\end{aligned} \tag{B.6}$$

The delta function operates on the left integral and right integral can be simplified to a product of delta functions $\delta_{p(l)\tilde{p}(l)}$ with index l:

$$\langle\Psi|\,\hat{n}_\uparrow(r)\,|\Psi\rangle = \frac{1}{N_\uparrow!}\sum_{p,\tilde{p}\in S_{N_\uparrow}}\mathrm{sign}(p)\,\mathrm{sign}(\tilde{p})\sum_{i=1}^{N_\uparrow}\psi^*_{n_{p(i)}}(r)\psi_{n_{\tilde{p}(i)}}(r)\prod_{l\neq i}\delta_{p(l)\tilde{p}(l)}. \tag{B.7}$$

If we set $p=\tilde{p}$ the product of delta functions will then assume the value 1 and $\mathrm{sign}(p)\,\mathrm{sign}(\tilde{p})$ can be simplified to $\mathrm{sign}^2(p)$. Otherwise, the expression is zero.

$$\langle\Psi|\,\hat{n}_\uparrow(r)\,|\Psi\rangle = \frac{1}{N_\uparrow!}\sum_{p\in S_{N_\uparrow}}\mathrm{sign}^2(p)\sum_{i=1}^{N_\uparrow}|\psi_{n_{p(i)}}(r)|^2 = \sum_{i=1}^{N_\uparrow}|\psi_{n_i}(r)|^2,\ \text{if } p=\tilde{p}. \tag{B.8}$$

The result in Eq. (B.8) can thus generalised for a given spin σ as

$$\langle \Psi | \, \hat{n}_\sigma(r) \, | \Psi \rangle = \sum_{i=1}^{N_\sigma} |\psi_{n_{\sigma i}}(r)|^2. \tag{B.9}$$

The probability density at position r is simply the sum of one-particle wave functions for one spin species.

C

Full Analytical Solution of Two Interacting Particles in One Dimension

The Hamiltonian for the two-particle system can be written as the sum of two single-particle Hamiltonians and an interaction potential

$$\hat{H} = -\frac{\hbar^2}{2m}\frac{\partial^2}{\partial x_1^2} - \frac{\hbar^2}{2m}\frac{\partial^2}{\partial x_2^2} + V_{pot}(x_1) + V_{pot}(x_2) + V_{int}(x_1 - x_2), \tag{C.1}$$

where

$$\begin{aligned} V_{pot}(x) &= \frac{1}{2}m\omega^2 x^2, \\ V_{int}(x) &= \alpha\delta(x). \end{aligned} \tag{C.2}$$

This Hamiltonian can be split into two parts, a centre-of-mass part and a relative part. To do this we define the variables

$$\begin{aligned} R &= \frac{1}{2}(x_1 + x_2), \\ r &= (x_1 - x_2), \\ x_1 &= R + \frac{1}{2}r, \\ x_2 &= R - \frac{1}{2}r, \end{aligned} \tag{C.3}$$

which means, by the chain rule, that

$$\begin{aligned} \frac{\partial^2}{\partial x_1^2} &= \frac{1}{4}\frac{\partial^2}{\partial R^2} + \frac{\partial^2}{\partial r^2} + \frac{\partial}{\partial r}\frac{\partial}{\partial R}, \\ \frac{\partial^2}{\partial x_2^2} &= \frac{1}{4}\frac{\partial^2}{\partial R^2} + \frac{\partial^2}{\partial r^2} - \frac{\partial}{\partial r}\frac{\partial}{\partial R}. \end{aligned} \tag{C.4}$$

Implementing these variables leads to the Hamiltonian

$$\begin{aligned} \hat{H} =& -\frac{\hbar^2}{2m}\frac{\partial^2}{\partial x_1^2} - \frac{\hbar^2}{2m}\frac{\partial^2}{\partial x_2^2} + \frac{1}{2}m\omega^2(x_1^2 + x_2^2) + \alpha\delta(x_1 - x_2) \\ =& -\frac{\hbar^2}{2m}\left(\frac{1}{4}\frac{\partial^2}{\partial R^2} + \frac{\partial^2}{\partial r^2} + \frac{\partial}{\partial r}\frac{\partial}{\partial R}\right) - \frac{\hbar^2}{2m}\left(\frac{1}{4}\frac{\partial^2}{\partial R^2} + \frac{\partial^2}{\partial r^2} - \frac{\partial}{\partial r}\frac{\partial}{\partial R}\right) \\ &+ \frac{1}{2}m\omega^2\left(\left(R + \frac{1}{2}r\right)^2 + \left(R - \frac{1}{2}r\right)^2\right) + \alpha\delta(r) \\ =& -\frac{\hbar^2}{2m}\left(\frac{1}{2}\frac{\partial^2}{\partial R^2} + 2\frac{\partial^2}{\partial r^2}\right) + \frac{1}{2}m\omega^2\left(2R^2 + \frac{1}{2}r^2\right) + \alpha\delta(r). \end{aligned} \tag{C.5}$$

We introduce the masses $M = 2m$ and $\mu = \frac{1}{2}m$ that are the total and reduced mass respectively and set $\hat{H}(R,r) = \hat{H}_{CoM}(R) + \hat{H}_{rel}(r)$. $\hat{H}_{CoM}(R)$ and $\hat{H}_{rel}(r)$ are defined as

$$\begin{aligned}\hat{H}_{CoM}(R) &= -\frac{\hbar^2}{2M}\frac{\partial^2}{\partial R^2} + \frac{1}{2}M\omega^2 R^2, \\ \hat{H}_{rel}(r) &= -\frac{\hbar^2}{2\mu}\frac{\partial^2}{\partial r^2} + \frac{1}{2}\mu\omega^2 r^2 + \alpha\delta(r).\end{aligned} \tag{C.6}$$

The first part, $\hat{H}_{CoM}$, is just a standard harmonic oscillator with eigenenergies $\hbar\omega(n+1/2)$, while $\hat{H}_{rel}$ looks like a one-dimensional QHO with a delta-function potential at the origin. We focus on solving the relative part. To continue, we define a harmonic oscillator length for the relative equation as

$$\lambda_{ho} = \sqrt{\frac{\hbar}{\mu\omega}} = \sqrt{2}\, l_{ho}, \tag{C.7}$$

where l_{ho} is the standard harmonic oscillator length. The equation is turned into its dimensionless form using the relation

$$r = \lambda_{ho}\xi \Rightarrow \frac{\partial^2}{\partial r^2} = \frac{1}{\lambda_{ho}^2}\frac{\partial^2}{\partial \xi^2} \tag{C.8}$$

and becomes

$$\begin{aligned}\hat{H}_{rel}(\xi) &= -\frac{\hbar^2}{2\mu}\frac{1}{\lambda_{ho}^2}\frac{\partial^2}{\partial\xi^2} + \frac{1}{2}\mu\omega^2(\lambda_{ho}\xi)^2 + \alpha\delta(\lambda_{ho}\xi) \\ &= -\frac{\hbar\omega}{2}\frac{\partial^2}{\partial\xi^2} + \frac{\hbar\omega}{2}\xi^2 + \frac{\alpha}{\lambda_{ho}}\delta(\xi).\end{aligned} \tag{C.9}$$

Here we redefine $\hat{H}_{rel}(\xi)$ as its dimensionless form by dividing it by the characteristic energy; i.e. we set $\hat{H}_r(\xi) = \hat{H}_{rel}(\xi)/\hbar\omega$.

$$\hat{H}_r(\xi) = -\frac{1}{2}\frac{\partial^2}{\partial\xi^2} + \frac{1}{2}\xi^2 + \frac{\alpha}{\hbar\omega\lambda_{ho}}\delta(\xi) = -\frac{1}{2}\frac{\partial^2}{\partial\xi^2} + \frac{1}{2}\xi^2 + \frac{\beta}{\sqrt{2}}\delta(\xi). \tag{C.10}$$

In the final step we define β as

$$\beta = \frac{\sqrt{2}\,\alpha}{\hbar\omega\lambda_{ho}} = \frac{\alpha}{\hbar\omega l_{ho}}. \tag{C.11}$$

With our new dimensionless expression $\hat{H}_r$, the time independent Schrödinger equation tells us

$$\hat{H}_r\Psi(\xi) = E\Psi(\xi) \Rightarrow \left(-\frac{1}{2}\frac{\partial^2}{\partial\xi^2} + \frac{1}{2}\xi^2 + \frac{\beta}{\sqrt{2}}\delta(\xi)\right)\Psi(\xi) = E\Psi(\xi), \tag{C.12}$$

where E is the eigenenergy. To solve this we need to express the unknown $\Psi(\xi)$ in terms of $\psi_n(\xi)$, the wave functions of the harmonic oscillator for a single particle corresponding to

$$\hat{H}_{QHO} = -\frac{1}{2}\frac{\partial^2}{\partial\xi^2} + \frac{1}{2}\xi^2. \tag{C.13}$$

In other words, we must expand $\Psi(\xi)$ in the basis of the free 1D-QHO states. This is done by a series expansion in terms of eigenstates which looks like

$$\Psi(\xi) = \sum_{n=0}^{\infty} c_n\psi_n(\xi). \tag{C.14}$$

By inserting this expression into equation (C.12) above we get

$$\begin{aligned}\left(-\frac{1}{2}\frac{\partial^2}{\partial\xi^2}+\frac{1}{2}\xi^2+\frac{\beta}{\sqrt{2}}\delta(\xi)\right)\sum_m c_m\psi_m(\xi)&=E\sum_n c_n\psi_n(\xi)\\ \sum_m c_m\left(-\frac{1}{2}\frac{\partial^2}{\partial\xi^2}+\frac{1}{2}\xi^2\right)\psi_m(\xi)+\sum_m c_m\psi_m(\xi)\frac{\beta}{\sqrt{2}}\delta(\xi)&=E\sum_n c_n\psi_n(\xi).\end{aligned} \tag{C.15}$$

Using the eigenenergies for the single-particle wave function $\hat{H}_{QHO}\psi_m(\xi) = E_m\psi_m(\xi)$ the expression becomes

$$\begin{aligned}\sum_m c_m E_m\psi_m(\xi)+\sum_m c_m\psi_m(\xi)\frac{\beta}{\sqrt{2}}\delta(\xi)&=E\sum_n c_n\psi_n(\xi)\\ \sum_m c_m E_m\psi_m(\xi)-E\sum_n c_n\psi_n(\xi)+\sum_m c_m\psi_m(\xi)\frac{\beta}{\sqrt{2}}\delta(\xi)&=0.\end{aligned} \tag{C.16}$$

We can express the QHO-term in either m or n, as it is just a series expression of $\Psi(\xi)$ in some variable. Thus, we replace m in the first term with n:

$$\begin{aligned}\sum_n c_n E_n\psi_n(\xi)-E\sum_n c_n\psi_n(\xi)+\sum_m c_m\psi_m(\xi)\frac{\beta}{\sqrt{2}}\delta(\xi)&=0\\ \sum_n c_n(E_n-E)\psi_n(\xi)+\frac{\beta}{\sqrt{2}}\delta(\xi)\sum_m c_m\psi_m(\xi)&=0.\end{aligned} \tag{C.17}$$

As a reminder, the energies E_n are the energies of the harmonic oscillator in equation (C.13), and E the energy from equation (C.12). The next step is calculating the coefficients c_n, which can be done by projecting equation (C.17) on $\psi_k^*(\xi)$, where k is some positive integer or zero, which gives

$$\begin{aligned}\int \mathrm{d}\xi\psi_k^*(\xi)\left(\sum_n c_n(E_n-E)\psi_n(\xi)+\frac{\beta}{\sqrt{2}}\delta(\xi)\sum_m c_m\psi_m(\xi)\right)&=0\\ \int \mathrm{d}\xi\sum_n c_n(E_n-E)\psi_n(\xi)\psi_k^*(\xi)+\frac{\beta}{\sqrt{2}}\int \mathrm{d}\xi\psi_k^*(\xi)\delta(\xi)\sum_m c_m\psi_m(\xi)&=0.\end{aligned} \tag{C.18}$$

The orthonormality of the wave function $\int \psi_k^*(x)\psi_n(x)\mathrm{d}x = \delta_{kn}$ and the operation of the delta function $\int \delta(x)f(x)\mathrm{d}x = f(0)$ turns the equation into

$$\begin{aligned}\sum_n c_n(E_n-E)\delta_{kn}+\frac{\beta}{\sqrt{2}}\psi_k^*(0)\sum_m c_m\psi_m(0)&=0\\ c_k(E_k-E)+\frac{\beta}{\sqrt{2}}\psi_k^*(0)\sum_m c_m\psi_m(0)&=0\\ c_k(E_k-E)+\frac{\beta}{\sqrt{2}}\psi_k^*(0)\Psi(0)&=0\\ \Rightarrow c_n=A\frac{\psi_n^*(0)}{E_n-E},&\end{aligned} \tag{C.19}$$

where $A=\frac{\beta}{\sqrt{2}}\Psi(0)$ is some normalisation constant. By reinserting this expression for c_n into the

second row of equation (C.19) again, we get

$$\begin{aligned} c_n(E_n - E) + \frac{\beta}{\sqrt{2}}\psi_n^*(0)\sum_m c_m\psi_m(0) &= 0 \\ A\psi_n^*(0) + A\frac{\beta}{\sqrt{2}}\psi_n^*(0)\sum_m \frac{\psi_m^*(0)\psi_m(0)}{E_m - E} &= 0 \\ 1 + \frac{\beta}{\sqrt{2}}\sum_m \frac{\psi_m^*(0)\psi_m(0)}{E_m - E} &= 0 \\ -\frac{1}{\beta} = \frac{1}{\sqrt{2}}\sum_m \frac{\psi_m^*(0)\psi_m(0)}{E_m - E} &= \frac{1}{\sqrt{2}}\sum_m \frac{|\psi_m(0)|^2}{E_m - E}. \end{aligned} \tag{C.20}$$

To continue we need to evaluate the sum. As $\hat{H}_{QHO}$ is a normal harmonic oscillator, with $\psi_m(\xi)$ being its wave functions, we can insert a known expression for it: equation (2.8), where we write $\widetilde{\psi}_m(\xi)$ as $\psi_m(\xi)$ for simpler notation.

$$\psi_m(\xi) = \frac{1}{\sqrt{2^m m!}}\frac{1}{\pi^{\frac{1}{4}}}e^{-\frac{\xi^2}{2}}H_m(\xi) \Rightarrow \psi_m(0) = \frac{H_m(0)}{\pi^{\frac{1}{4}}\sqrt{2^m m!}}. \tag{C.21}$$

Similarly, the energies E_m of the harmonic oscillator in terms of the characteristic energy is also known as $(m + \frac{1}{2})$; However, for odd m, the wave function in $\xi = 0$ becomes zero due to the Hermite polynomial and the solution becomes trivial. The physical interpretation of this would be that states with an odd relative wave function cannot interact through the delta potential V_{int}. To eliminate the redundant parts, we use the variable substitution $m = 2n$. With this substitution, we get

$$\psi_{2n}(0) = \frac{H_{2n}(0)}{\pi^{\frac{1}{4}}\sqrt{2^{2n}(2n)!}}, \tag{C.22}$$

and $E_{2n} = (2n + \frac{1}{2})$. Inserting these expressions for ψ_{2n} and E_{2n} into equation (C.20) we get

$$\frac{1}{\sqrt{2}}\frac{|\psi_{2n}(0)|^2}{E_{2n} - E} = \frac{1}{\sqrt{2\pi}}\frac{(H_{2n}(0))^2}{(2^{2n}(2n)!)(2n + \frac{1}{2} - E)} = \frac{1}{2\sqrt{2\pi}}\frac{1}{2^{2n}}\frac{\frac{(H_{2n}(0))^2}{(2n)!}}{n - (\frac{E}{2} - \frac{1}{4})}. \tag{C.23}$$

By letting $\left(\frac{E}{2} - \frac{1}{4}\right) = \nu$, we can use an integral substitution:

$$\frac{1}{n - \nu} = \int_0^\infty \frac{\mathrm{d}x}{(1+x)^2}\left(\frac{x}{1+x}\right)^{n-\nu-1}. \tag{C.24}$$

Our expression for $-1/\beta$ now reads

$$\begin{aligned} -\frac{1}{\beta} = \frac{1}{\sqrt{2}}\sum_n \frac{|\psi_{2n}(0)|^2}{E_{2n} - E} &= \frac{1}{2\sqrt{2\pi}}\sum_n \frac{1}{2^{2n}}\frac{\frac{(H_{2n}(0))^2}{(2n)!}}{n - \nu} \\ &= \frac{1}{2\sqrt{2\pi}}\sum_n \int_0^\infty \frac{\mathrm{d}x}{(1+x)^2}\left(\frac{x}{1+x}\right)^{n-\nu-1}\frac{1}{2^{2n}}\frac{(H_{2n}(0))^2}{(2n)!}. \end{aligned} \tag{C.25}$$

The reason for doing this substitution is to use the generating function for the squared Hermite polynomial [13, p. 250]. It says that

$$\sum_n \frac{(H_{2n}(x))^2}{(2n)!}\left(\frac{z}{2}\right)^{2n} = \frac{\exp\left(\frac{2x^2 z}{1+z}\right)}{\sqrt{1-z^2}} \Rightarrow \sum_n \frac{(H_{2n}(0))^2}{(2n)!}\left(\frac{z}{2}\right)^{2n} = \frac{1}{\sqrt{1-z^2}}. \tag{C.26}$$

To get rid of all n-dependence, we want z to be $\sqrt{\frac{x}{1+x}}$, which can be achieved by reordering the terms.

$$\begin{aligned}
&\frac{1}{2\sqrt{2\pi}}\sum_n \int_0^\infty \frac{\mathrm{d}x}{(1+x)^2}\left(\frac{x}{1+x}\right)^{n-\nu-1}\frac{1}{2^{2n}}\frac{(H_{2n}(0))^2}{(2n)!}\\
&\quad=\frac{1}{2\sqrt{2\pi}}\int_0^\infty \frac{\mathrm{d}x}{(1+x)^2}\left(\frac{x}{1+x}\right)^{-\nu-1}\sum_n\left(\frac{x}{1+x}\right)^{n}\frac{1}{2^{2n}}\frac{(H_{2n}(0))^2}{(2n)!}\\
&\quad=\frac{1}{2\sqrt{2\pi}}\int_0^\infty \frac{\mathrm{d}x}{(1+x)^2}\left(\frac{x}{1+x}\right)^{-\nu-1}\sum_n\left(\frac{1}{2}\sqrt{\frac{x}{1+x}}\right)^{2n}\frac{(H_{2n}(0))^2}{(2n)!}.
\end{aligned} \tag{C.27}$$

Now we use equation (C.26) to get

$$\begin{aligned}
-\frac{1}{\beta}&=\frac{1}{2\sqrt{2\pi}}\int_0^\infty \frac{\mathrm{d}x}{(1+x)^2}\left(\frac{x}{1+x}\right)^{-\nu-1}\left(1-\left(\frac{x}{1+x}\right)\right)^{-1/2}\\
&=\frac{1}{2\sqrt{2\pi}}\int_0^\infty \frac{\mathrm{d}x}{(1+x)^2}\left(\frac{x}{1+x}\right)^{-\nu-1}\left(\frac{1}{1+x}\right)^{-1/2}\\
&=\frac{1}{2\sqrt{2\pi}}\int_0^\infty \mathrm{d}x\left(\frac{x}{1+x}\right)^{-\nu-1}\left(\frac{1}{1+x}\right)^{3/2}\\
&=\frac{1}{2\sqrt{2\pi}}\int_0^\infty \mathrm{d}x\,(x)^{-\nu-1}\left(\frac{1}{1+x}\right)^{-\nu-1}\left(\frac{1}{1+x}\right)^{3/2}\\
&=\frac{1}{2\sqrt{2\pi}}\int_0^\infty \mathrm{d}x(x)^{-\nu-1}\,(1+x)^{-1/2+\nu}\,.
\end{aligned} \tag{C.28}$$

Here, we can rewrite this concisely using the integral representation of Tricomi's confluent hypergeometric function U [14, p. 505]:

$$\Gamma(a)U(a,b,z)=\int_0^\infty \mathrm{d}t e^{-zt}t^{a-1}(1+t)^{b-a-1}. \tag{C.29}$$

By inspecting each variable we can see that z is 0, a is $-\nu$, and b is $\frac{1}{2}$. Thus we can rewrite equation (C.28) as

$$-\frac{1}{\beta}=\frac{1}{2\sqrt{2\pi}}\int_0^\infty \mathrm{d}x(x)^{-\nu-1}(1+x)^{-1/2+\nu}=\frac{1}{2\sqrt{2\pi}}\Gamma\left(-\nu\right)U\left(-\nu,\frac{1}{2},0\right). \tag{C.30}$$

This representation is initially only valid for $\nu<0$, which would severely limit its usefulness, but with analytic continuation this problem is removed for all $E\neq E_n$ [11]. According to [14, p. 504], Tricomi's confluent hypergeometric function can be written

$$U(a,b,0)=\frac{\pi}{\sin(\pi b)}\frac{M(a,b,0)}{\Gamma(1+a-b)\Gamma(b)}, \tag{C.31}$$

Where M is Kummer's confluent hypergeometric function. $M(a,b,z)$ can be expressed as a series expansion in z, which makes the first term of said expansion $M(a,b,0)$.

$$M(a,b,z)=1+\frac{az}{b}+O(z^2)\Rightarrow M(a,b,0)=1. \tag{C.32}$$

Thus we get

$$\begin{aligned}
U(-\nu,\frac{1}{2},0)&=\frac{\pi}{\sin\left(\pi\frac{1}{2}\right)}\frac{1}{\Gamma(1-\nu-\frac{1}{2})\Gamma(\frac{1}{2})}\\
&=\frac{\pi}{\Gamma(\frac{1}{2}-\nu)\Gamma(\frac{1}{2})}=\frac{\sqrt{\pi}}{\Gamma(\frac{1}{2}-\nu)}.
\end{aligned} \tag{C.33}$$

Finally, by inserting this expression for U into equation (C.30) we get

$$
\begin{aligned}
-\frac{1}{\beta} &= \frac{1}{2\sqrt{2\pi}}\Gamma(-\nu)U\left(-\nu,\frac{1}{2},0\right) \\
&= \frac{1}{2\sqrt{2}}\frac{\Gamma(-\nu)}{\Gamma(\frac{1}{2}-\nu)} \\
&= \frac{1}{2\sqrt{2}}\frac{\Gamma\left(-\left(\frac{E}{2}-\frac{1}{4}\right)\right)}{\Gamma\left(\frac{1}{2}-\left(\frac{E}{2}-\frac{1}{4}\right)\right)} \\
&= \frac{1}{2\sqrt{2}}\frac{\Gamma\left(-\frac{E}{2}+\frac{1}{4}\right)}{\Gamma\left(-\frac{E}{2}+\frac{3}{4}\right)}.
\end{aligned}
\tag{C.34}
$$

Thus we have a function $\beta(E)$, linking the interaction strength with the relative energy of the system:

$$
\beta(E) = -2\sqrt{2}\frac{\Gamma\left(-\frac{E}{2}+\frac{3}{4}\right)}{\Gamma\left(-\frac{E}{2}+\frac{1}{4}\right)}. \tag{C.35}
$$

By inverting this function numerically, we can find the energy as a function of interaction strength, $E(\beta) = E(\alpha/l_{ho}\hbar\omega)$.

DEPARTMENT OF PHYSICS
CHALMERS UNIVERSITY OF TECHNOLOGY, UNIVERSITY OF GOTHENBURG
Gothenburg, Sweden
www.chalmers.se

CHALMERS